Title: The BR-body proteome contains a complex network of protein-protein and protein-RNA interactions

Authors: Nandana, V.[1]#, Rathnayaka-Mudiyanselage, I.W.[1,2]#, Muthunayake, N.S.[1*], Hatami, A.[3] Mousseau, C.B.[4], Ortiz-Rodríguez, L.A.[5], Vaishnav, J.[3$], Collins, M.[6], Gega, A.[1&], Mallikaarachchi, K.S.[1], Yassine, H.[1], Ghosh, A.[1], Biteen, J.S.[5], Zhu, Y.[3], Champion, M.M.[4], Childers, W.S.[6], Schrader, J.M.[1]

[1]Wayne State University, Department of Biological Sciences, Detroit, MI

[2]Wayne State University, Department of Chemistry, Detroit, MI

[3]Wayne State University, Department of Chemical Engineering and Materials Science, Detroit, MI

[4]University of Notre Dame, Department of Chemistry, Notre Dame, IN

[5]University of Michigan, Department of Chemistry, Ann Arbor, MI

[6]University of Pittsburgh, Department of Chemistry, Pittsburgh, PA

[#]These authors contributed equally

[&]Current affiliation: University of Toledo Medical School

[$]Current affiliation: University of Massachusetts-Amherst

*Current affiliation: Wayamba University of Sri Lanaka, Faculty of Medicine, Department of Biochemistry

Corresponding Author: Schrader@wayne.edu

Highlights

1. BR-body proteomics identified 111 proteins enriched in BR-bodies.
2. BR-bodies associate with an interconnected network of RNP condensates.
3. BR-body condensation is modulated by its interaction network.
4. RNA is required for rapid BR-body condensation.

Abstract

Bacterial RNP bodies (BR-bodies) are non membrane-bound structures that facilitate mRNA decay by concentrating mRNA substrates with RNase E and the associated RNA degradosome machinery. However, the full complement of proteins enriched in BR-bodies has not been defined. Here we define the protein substrates of BR-bodies through enrichment of the bodies followed by liquid chromatography-mass spec (LC-MS) proteomic analysis. We found 111 BR-body enriched proteins, including many RNA binding proteins, many of which are also recruited directly to *in vitro* reconstituted RNase E droplets, suggesting BR-bodies are more complex than previously assumed. While most BR-body enriched proteins cannot phase separate, we identified five which can undergo RNA dependent phase separation *in vitro*, suggesting other RNP condensates interface with BR-bodies. The RNA degradosome protein clients are recruited more strongly to RNase E droplets than that of the other RNP condensates, suggesting that client specificity is largely achieved through direct protein-protein interactions. We observe that some RNP condensates assemble unidirectionally, suggesting that RNA may be trafficked through RNP condensates in an ordered manner to facilitate mRNA processing/decay, and that some BR-body associated proteins have the capacity to dissolve the condensate. Finally, we find that RNA dramatically stimulates the rate of RNase E phase separation *in vitro*, explaining the observed dissolution of BR-bodies after cellular mRNA depletion observed previously. Altogether, these results suggest that a complex network of protein-protein and protein-RNA interactions controls BR-body phase separation while coordinating this mode of organization with RNA processing.

Introduction:

Biomolecular condensates have shown to be an important mode of subcellular organization in eukaryotes and bacteria[1–3]. As bacteria often lack membrane bound organelles, biomolecular condensates may provide a generalized strategy to their subcellular organization. Indeed, many bacterial biomolecular condensates have been recently identified in various species, including BR-bodies, signaling condensates, DNA replication condensates, RNApol condensates, Hfq condensates, Rubisco condensates, etc.[4–10]. Biomolecular condensates typically assemble through the physical process of phase-separation, which involves association of macromolecular scaffolds and segregation of other cellular components, ultimately leading to distinct non-membrane bounded structures[11]. Recent analyses of condensate physical properties appear to be consistent with a model of percolation-coupled phase separation, which includes both associative interactions as well as segregative[12] leading to phase separation[13]. Macromolecules which have the capacity to phase separate are referred to as scaffolds, which generally provide a platform for multi-valent interactions leading to phase separation and molecules that are recruited to condensates but cannot phase separate themselves are called clients[14] with the composition of scaffolds and clients that make up a condensate will determine the biochemical and cellular function. Importantly, molecules inside of condensates can often show diffusive dynamics, suggesting biomolecular condensates can facilitate biochemical processes within them[15,16]. Models have been suggested for how condensates might help accelerate enzyme catalyzed processes, including acceleration of reaction rates by local concentration, increased reaction specificity by selective recruitment of certain substrates and avoidance of others, and the ability to prevent release of pathway intermediates[17–19]. Conversely, they have been proposed to sequester substrate molecules from their enzymes leading to a reduction in reaction rates[20,21]. To determine the biochemical consequences of biomolecular condensate organization, an important goal is to be able to purify and reconstitute the essential molecular components of the condensate.

Despite advances in biomolecular condensate biochemistry, many *in vitro* studies have focused on purified scaffolds, and often lack the full suite of molecules identified to interact *in vivo*. This is potentially problematic, as proteomic/transcriptomic investigations of eukaryotic biomolecular condensates have revealed that biomolecular condensates are enriched in hundreds of different molecular species that may alter their biochemical or cellular functions. For example, P-bodies have been found to have >125 proteins and >6000 RNA transcripts[22], and importantly appear to help concentrate mRNA decay enzymes (including decapping enzymes, LSM proteins, Xrn1 nuclease, deadenylases, etc.) together with decapped translationally repressed mRNAs. Stress granules have been found to contain >300 proteins and >1800 RNA transcripts[23–25], often including a partially overlapping set of components with P-bodies[22,26], yet the differences in composition and slower dynamics[27] suggests that these structures likely have distinct functions. Through careful quantitative measurements, the core set of P-body proteins has recently been reconstituted *in vitro*, with similar dynamic propertiess[28]. In bacteria, BR-bodies were found to be enriched in long, poorly translated cellular mRNAs and sRNAs, a class of translational repressors, together with the RNA degradosome proteins[4,29]. Therefore, it was assumed that this structure might have a small set of protein clients that could be amendable to full *in vitro* reconstitution, however, the full complement of proteins in BR-bodies were not defined[27].

To define the proteome of *Caulobacter crescentus* BR-bodies, we performed a cellular enrichment by differential centrifugation[30] followed by quantitative liquid chromatography tandem mass

spectrometry (LC-MS). Similar to eukaryotic condensates, we identified over 100 proteins which were enriched in BR-bodies. Enriched proteins tend to localize into foci *in vivo* and enter RNase E condensates *in vitro*, suggesting many are likely direct clients of RNase E, the main scaffold of the BR-body. While most enriched proteins do not assemble into biomolecular condensates *in vitro*, we identified five BR-body associated proteins which can undergo phase-separation (phase separate without RNase E), suggesting they form distinct RNP condensates in the cell that interact with RNase E. By assaying the pairwise ability of each scaffold protein to mix with the others, we observed that some pairs of scaffolds have strong associations, and that certain pairs show directional recruitment which likely impacts RNP assembly order, leading to heterogenous RNP condensates *in vivo*. We also identified two proteins which can dissolve BR-bodies both *in vivo* and *in vitro*, suggesting that they may negatively regulate the cell's ability to assemble BR-bodies. Despite the identification of many BR-body associated proteins, the RNA degradosome proteins are the only proteins identified that stoichiometrically bind to RNase E[31], suggesting a minimal BR-body may be possible to reconstitute. Minimal BR-body phase separation was kinetically stimulated by RNA, and showed similar RNase E FRAP dynamics to RNase E-RNA droplets. Overall, this suggests that BR-bodies have similar complex interaction network to eukaryotic RNP condensates, and the reconstitution of the "core" minimal BR-body components provides an exciting framework to begin assessing their biochemical functions and how they might be altered by the addition of BR-body associated proteins.

Results

LC-MS Proteomics to characterize the BR-body proteome

In order to define the *C. crescentus* BR-body associated proteome, BR-body enrichment was performed as in[30] and subjected to bottom-up proteomics preparation and analysis (Fig 1A). Here we compared enriched BR-body samples to a mock treated lysate using a mutant that is unable to assemble BR-bodies due to the deletion of the C-terminal IDR of RNase E[30]. 100 μg protein was prepared in triplicate for either condition and converted into peptides via enzymatic digestion using S-Traps[32]. Each sample was analyzed by LC-MS/MS in technical triplicate. Peptide-spectral matching, protein inference and Label Free Quantification (LFQ) was performed using FlashLFQ in MetaMorpheus[33]. Data were filtered to an FDR of 1.0% and exported as text for analysis. Using these parameters, a total of 1079 proteins were identified in both samples, and the ratio of signal in the BR-body enriched sample (JS299) over the negative control (JS221) was plotted (Fig 1B). 111 proteins were identified to be enriched in BR-bodies. These enriched proteins had Log2 BR-body enrichment value of >1 (>2-fold enrichment) with a >95% confidence interval (resulting p-values subject to Benjamini-Hochberg correction) or were identified in all three biological replicates in BR-body enriched samples but were not detected in the negative control. These enriched proteins were predominantly cytoplasmic, while proteins derived from other cellular compartments were depleted, suggesting reasonable enrichment of BR-bodies occurred in the sample. In addition, we observed significantly higher scores for known RNase E associated proteins, while proteins that interact with polar biomolecular condensates were highly depleted (Fig 1B), suggesting that the enrichment is likely not contaminated with all cellular condensates. Of all the enriched proteins, go-term enrichment found proteins with RNA binding, ATP binding, GTPase activity, or RNA degradation functionalities (Fig 1B). To validate whether BR-body enriched proteins localize into BR-bodies *in vivo*, we expressed a set of YFP-tagged proteins that were enriched in BR-bodies together with a set of other RNA related proteins that were not enriched in BR-bodies from the vanillate locus (Fig S1) and determined the average number of foci/cell (Fig 1C). Interestingly, 7/11 proteins from the

BR-body enriched set assembled into foci in the cells, while only 3/11 proteins from the negative control set showed foci. Amongst the 4 known BR-body clients we found that 3/4 were enriched within these assemblies. RNase D1 was found to be RNase E associated[34] and showed foci within cells, however, was depleted in the BR-body proteomics data. Of the 4/11 proteins that were enriched but did not form foci, it is possible that the C-terminal YFP tag might interfere with their ability to form foci, as SmpB which was found to form foci by immunofluorescence[35] and did not form foci when fused to YFP. Interestingly, MetK has been found to form foci previously[36] and RNase HI may be associated with the replisome foci, so both of these foci are unlikely to be BR-bodies, and likely represent other structures. Overall, the larger abundance of foci in the BR-body enriched set suggest the BR-body enriched proteomic data represents many true-positive BR-body associated proteins with limited false-positives.

Identification of BR-body associated scaffolds that condense independent of RNase E

Since the C-terminal IDR of RNase E was found to be necessary and sufficient to form BR-bodies, we tested whether RNase E was required for BR-body enriched proteins to form foci (Fig 2). Since RNase E is essential, we used an RNase E depletion strain where the sole copy of RNase E is under control of the xylose promoter[4]. While most proteins maintained similar YFP fluorescence, RhlB, Aconitase, PNPase, and RNase H1-YFP proteins were expressed at levels that were too low to detect in the depletion strain. To overcome low expression for aconitase, we utilized a different strain in the lab used previously in which Aconitase-YFP was present at its native loci in the same xylose dependent RNase E depletion strain[4]. We observed and quantified foci for each of the YFP fusions, however, RNase D1 appeared to show localization to the inner membrane with a lower number of foci as compared to the other strains tested. For Aconitase, RNase D1, Hfq, and Rho, fluorescent foci levels dropped significantly upon RNase E depletion, suggesting that these proteins likely require RNase E to assemble into foci. Interestingly, for MetK and RhlE, foci levels were similar or higher upon RNase E depletion, suggesting that these two proteins assemble into foci independent of RNase E.

As MetK and RhlE proteins were identified to assemble RNase E independent foci *in vivo*, we tested whether these proteins could directly self-assemble into condensates *in vitro*. In addition to MetK and RhlE, we also included several additional proteins from the BR-body enrichment dataset or which were known to interact with RNase E (Figs 3, S2A). Each protein was incubated near their estimated *in vivo* concentration[37], and was incubated with or without 20 ng/µL of *C. crescentus* total RNA. We identified that RhlE, DeaD, Hfq, MetK, and FabG all assembled RNA stimulated condensates *in vitro* (Figs 3A, B), suggesting that these proteins are scaffolds that can drive RNA dependent condensation. Conversely, a majority of the proteins tested including PNPase, Aconitase, RhlB, RNase D1, ribosomal protein S1, NudC, RppH, Rho, NusG, DnaK, and tyrosyl tRNA synthetase (TyrRS) did not undergo phase separation regardless of the presence of RNA (Fig S2B). Consistent with the phase-separation of RhlE, DeaD, and Hfq, the homologous proteins from *E. coli* were recently found to assemble into condensates *in vitro* or when overexpressed *in vivo*[7,38]. To test whether these structures are condensates, we performed high-salt and RNase treatment (Fig 3C), and in each case all the structures were strongly dissociated, suggesting multivalent electrostatic interactions with RNA are likely important for driving phase separation, like in RNase E condensates[4]. RhlE, DeaD, and Hfq contain intrinsically disordered regions (IDRs) (Fig 3A) that have been characterized as important for their *E. coli* homologues to be able to form droplets[38,39]. Prior experiments also showed that the IDR of RNase E was both necessary and sufficient for phase separation[4]. To test the function of these IDRs on phase-separation we deleted the IDRs of *C. crescentus* RhlE, DeaD, and Hfq and tested for their ability to phase-separate and found that

for Hfq and DeaD the IDR deletions showed reduced phase-separation, while for RhlE the IDR deletion was indistinguishable from wild-type (Fig S2C). We did not include FabG and MetK in these experiments as no disordered regions were predicted in their sequences (Fig 3A). Overall, this suggests that for some of these scaffold proteins, IDRs provide a positive influence of phase separation, but are not strictly required for phase separation.

A complex network of molecular interactions regulates RNP condensate

To better understand which proteins can enter BR-bodies, we selected a set of 18 proteins (Fig S2A) to test further for their recruitment directly into RNase E droplets (Fig 4A). We picked proteins enriched from the BR-body proteomics dataset with known RNA-processing roles, proteins known to have protein-protein interactions with RNase E but not detected in the BR-body proteomics experiment, as well as negative control proteins with low BR-body enrichment and no known/predicted interaction. In these experiments RNase E and RNA were added to form an RNase E condensate, followed by the incubation of a Cy5 labeled test protein. The partition coefficient was calculated from the images for each protein assayed based on the Cy5 fluorescence (Figs 4B, S4A). Here we observed that the core RNA degradosome proteins PNPase, Aconitase, RhlB, and RNase D1 all had positive partition coefficients ranging from 2.7 to 4.7 showing they enter RNase E condensates, while our negative controls of BSA or, SpmX which forms a polar signaling condensate[6], did not enter and yielded a partition coefficient near 1 indicating no enrichment. We also identified partition coefficients at similar levels to the core degradosome proteins for RhlE, DnaK, and FabG. In contrast NudC, RppH, Rho, NusG, and TyrRS all contained partition coefficients close to 1, similar to the negative control BSA and SpmX (Fig 4B). The low partition coefficients for RppH and NudC are consistent with their lack of enrichment in the BR-body proteomics assay, however, Rho, NusG, and TyrRS all had significant enrichment in the BR-body proteomics data suggesting they may enter BR-bodies indirectly through another protein. Despite the finding that many proteins were able to enter BR-bodies, none of these proteins altered the partition coefficient of RNase E (Fig S3B), suggesting that a majority of BR-body associated proteins are not dramatically influencing RNase E's condensation.

As some BR-body proteins were found to assemble into RNA dependent condensates on their own, we tested which BR-body associated proteins might induce condensation in the absence of RNA (Fig S4). To test each client's ability to stimulate RNase E condensation, we added each protein at their in-vivo concentration[37]. Interestingly, we found that PNPase, RhlB, and RhlE stimulated RNase E condensates rather robustly in the absence of RNA (Fig S4A). In addition, FabG and Hfq stimulated irregularly shaped condensates in the absence of RNA while Aconitase, RNase D1, NudC, RppH, Rho, NusG, DnaK, TyrRS, ribosomal protein S1, and MetK did not stimulate RNase E condensation (Fig S4A). This suggests that a subset of BR-body associated proteins can stimulate condensation independent of RNA.

Interestingly, we observed that the addition of ribosomal protein S1 (RpsA) or MetK, which were not BR-body enriched (Table S1) but were previously found to associate with RNase E via CoIP[40], could dissolve RNase E droplets *in vitro* (Figs 4A,5A). Ribosomal protein S1 could only dissociate the droplets if the condensates contained total RNA, while MetK showed strong dissolution if RNase E was condensed with RNA or with the protein PNPase. To test whether the differences between S1 and MetK were related to their inherent RNA binding interactions, we examine the apparent binding on 9s rRNA, a known RNase E substrate[31]. Based on the native gel shifts we found that ribosomal protein S1 bound

RNA with tighter apparent affinity than MetK (Fig 5B). The tighter apparent affinity with RNA may explain why ribosomal protein S1 preferentially dissolves RNase E condensates in the presence of RNA. We also used a coIP assay with MBP-RNase E to test MetK and ribosomal protein S1 association with MBP-RNase E. Indeed, as compared to the core BR-body protein aconitase which is thought to stoichiometrically bind to RNase E[30], we found that both ribosomal protein S1 and MetK showed lower CoIP than aconitase. However, MetK showed a faint band of protein retained on the resin, while ribosomal protein S1 showed no detectable retention (Fig 5C). Overall, these data suggest that MetK dissociates BR-bodies through interactions with the RNase E protein (Fig 5). To examine whether this observed *in vitro* dissolution effect is relevant *in vivo*, we inserted the ribosomal protein S1 and *metK* genes into the pBXMCS-2 overexpression vector[41] and transformed the plasmid into a strain harboring a tagged BR-body marker (Aconitase-mCherry)[4]. We observed *in vivo* that both MetK and ribosomal protein S1 overexpression strongly reduced Aconitase-mCherry foci (Fig 5D), confirming that their dissolution of BR-bodies observed *in vitro* can also occur *in vivo*.

As some BR-body enriched proteins were able to assemble into RNP condensates independent of RNase E (Fig 4B), the client specificity of these RNP condensates was unknown. As the RNA degradosome client proteins are known to be stoichiometrically bound to RNase E via direct protein-protein interaction sites[31,40], we tested the specificity of each driver/scaffold to each core RNA degradosome protein labeled with Cy5 dye (Fig 6A). Here we observed a larger partition coefficient for all Cy5 degradosome clients to RNase E condensates as compared to any of the other scaffolds/drivers (Figs 6A, S4B), suggesting that the degradosome proteins have a specificity for RNase E condensates, likely through their protein-protein interactions.

Next, the miscibility of the scaffolds/drivers of each single RNP condensate was examined (Fig 6B). First, we pre-formed a condensate using an unlabeled scaffold and then added in a Cy5 labeled scaffold in all pairwise combinations and assayed the partition coefficients. We induced condensation in the presence or absence of RNA to test the RNA dependency of each interaction. In the presence of RNA we assayed condensate formation using the predicted *in vivo* protein concentrations[37], and in the absence of RNA condensates were stimulated by increasing the protein concentration above its *in vivo* concentration. For the RNase E condensate, we observed similar recruitment of other scaffolds regardless of whether the condensates were formed with RNA or protein only (Figs 6B, S4B). The partition coefficients for these scaffolds into RNase E condensates tracked with the BR-body enrichment measured previously. RhlE was recruited strongest into the RNase E condensate (11 partition coefficient) and had the highest observed BR-body enrichment (10 fold), while Hfq (7.5 partition coefficient, 3.2 BR-body enrichment), FabG (3.8 partition coefficient, 2.2 fold BR-body enrichment), and DeaD (1.5 partition coefficient, 1.6 fold BR-body enrichment). For RhlE, we observed that it was recruited strongly into other RNP condensates, with partition coefficients ranging from 4.3 to 11, while the other scaffolds were recruited poorly into RhlE-RNA condensates, with partition coefficients ranging from 1.5 to 2.5. In the absence of RNA, RhlE strongly recruited RNase E (12) or DeaD (9.8) while Hfq and FabG maintained similar partition coefficients (Fig S4B). DEAD condensates showed strong recruitment of RhlE and lower recruitment of the other scaffolds, with subtle changes in the presence or absence of RNA. While RhlE and FabG were similarly recruited to Hfq condensates regardless of the presence of RNA, RNase E dissolved Hfq-RNA condensates while Hfq protein only condensates strongly recruited RNase E (6.9 partition coefficient) while DEAD was recruited at a low level in Hfq-RNA condensates (1.8 partition coefficient) and dissolved Hfq only condensates. FabG condensates only formed in the

presence of RNA and showed strongest recruitment of RhlE (7.4) and Hfq (3.4). In summary, the scaffold proteins which assemble diverse RNP condensates show specificity of recruitment, suggesting that some RNP condensates can intermix, while others likely do not.

The asymmetric recruitment/dissolution (Fig 6B) and specificity of clients (Fig 6A) observed may help shape the composition of heterogeneous RNP condensates in the cell. We chose to study RhlE-RNase E pair further because it showed the strongest directional recruitment in the presence of RNA (Fig 6B). First, we altered the order of addition of RhlE and RNase E in which we could either mix both proteins together before triggering phase separation (Fig 6C). If the proteins are mixed before condensation with RNA, we observed that RNase E and RhlE mix uniformly. We also changed the order of addition and pre-assembled each protein into condensates with RNA before mixing both RNP condensates together (Fig 6C). When each protein was pre-assembled into a condensate, we observed that RNase E and RhlE condensates did not readily mix with each other. This contrasts with the prior observation that free RhlE readily entered RNase E condensates (Fig 6B), suggesting that the order of assembly influences the composition of these RNase E and RhlE condensates.

To test whether RhlE forms condensates separate from BR-bodies *in vivo*, we coexpressed RhlE-YFP together with Aconitase-mCherry (a marker for BR-bodies) and imaged them in the same cells (Fig 6D). As a control, we imaged RNase E-YFP together with Aconitase-mCherry, which are known to strongly colocalize[4]. In general, we observed a heterogeneous mixture of RhlE foci, RNase E foci, and mixed RhlE/RNase E foci. For each YFP focus we observed, we drew line traces and calculated the Pearson correlation between the YFP and mCherry channels across the line trace. The RNase E signal was strongly colocalized with Aconitase-mCherry (R=0.9), and for a strain lacking YFP, we found that the correlation between YFP autofluorescence and Aconitase-mCherry was near zero. Interestingly, we observed that RhlE and Aconitrase had an intermediate correlation (R=0.4), with some RhlE foci strongly correlating with Aconitase, and other RhlE foci totally lacking Aconitase (Fig 6D). In addition to colocalization, we also examined the assembly order of RNase E and RhlE condensates formation *in vivo* with taking time-lapse movies of cells. To do this, we took time-lapse movies of cells and examined the order of RhlE and RNase E foci formation in cells. As a positive control, we observed that RNase E-YFP and Aconitase-mCherry foci appear simultaneously (Fig 6E, S5A). When BR-bodies appear first, as indicated by Aconitase-mCherry foci, we consistently observed RhlE-YFP signal within these foci (Fig 6E), consistent with the ability of RNase E condensates to recruit RhlE *in vitro* (Fig 6B). In contrast, RhlE-YFP foci that appeared first generally lacked a colocalized Aconitase-mCherry focus, also consistent with the lack of *in vitro* recruitment (Fig 6B). Taken altogether, these observations suggest that the network of interactions driving RhlE and RNase E condensation likely controls the ability of these condensates to coassemble and mix both *in vitro* and *in vivo*. To further test how the network of interactions affects the condensates, we performed *in vitro* FRAP on RhlE and RNase E droplets (Fig S5B). We observed that RNase E rapidly recovers either in RNase E-RNA condensates or in mixed RNase E-RhlE-RNA condensates, while RhlE showed little to no recovery in RhlE-RNA condensates or RNase E-RhlE-RNA condensates (Fig S5B). To test whether RhlE ATPase activity might influence its dynamics, we found the addition of ATP-Mg^{2+} did not alleviate RhlE recovery (Fig S5B). Overall, this suggests that the material properties of RhlE-RNA and RNase E-RNA condensates contribute to the unidirectional mixing observed *in vitro* and *in vivo*.

As RNase E did not appear to readily enter other associated RNP condensates (Fig 6A), we wanted to better understand the role of RNA and the associated degradosome proteins on its

condensation. We therefore examined the kinetics of condensation via time-lapse microscopy (Fig 7A, 7B). This assay likely reflects the kinetic processes of phase-separation and surface wetting of the microscope slide. When incubated alone at its predicted *in vivo* concentration, RNase E did not phase separate *in vitro* even after long incubations of several minutes. RNase E was able to phase separate without RNA after prolonged incubation of many minutes, and at concentrations much higher than its predicted *in vivo* concentration the extent of phase separation was enhanced (Fig S6). The addition of RNA strongly stimulated the rate of condensation, occurring on the sub-minutes timescale, consistent with the known importance of RNA for condensation *in vivo* and in end-point *in vitro* assays[4,29]. Importantly though, RNase E is known to scaffold the RNA degradosome protein complex, and the degradosome proteins stoichiometrically bind to RNase E[31] and are homogeneously present with RNase E in BR-bodies[4]. To test the effects of degradosome proteins on condensation kinetics, we added either PNPase or the full set of core degradosome proteins (PNPase, Aconitase, RhlB, and RNase D1) to the condensation assembly experiment. The addition of PNPase or the full set of core RNA degradosome proteins still allowed for rapid RNA stimulated condensation on the sub-minute timescale. This suggests that the combined interactions with the RNA degradosome proteins likely do not dramatically alter RNase E's condensation kinetics in the presence of RNA. This may be due to the degradosome protein binding sites being located outside the Arg-rich RNA binding sites in the C-terminal domain[31]. As noted previously, we observed that the degradosome protein PNPase was able to stimulate RNase E condensation *in vitro* in the absence of RNA (Fig S4A). We therefore assayed the kinetics of RNase E PNPase condensation in the absence of RNA and found that the kinetics were dramatically slower than in the presence of RNA. Overall, this suggests that RNA provides the strongest stimulation in condensation, and the RNA degradosome clients can provide a slight further enhancement in RNA-mediated condensation.

To understand if RNA or degradosome protein interactions alter the mobility of molecules in the condensed state, we performed FRAP experiments (Fig 7C). RNase E condensates lacking RNA had the slowest recovery, at 2.4 min $\tau_{1/2}$, while the addition of RNA accelerated the FRAP recovery $\tau_{1/2}$to 0.23 [27]min. Interestingly, the addition of PNPase and RNA, or all degradosome proteins and RNA showed fast mobility between 0.34 and 0.42 min $\tau_{1/2}$, similar to the RNase E with RNA sample. This suggests that the addition of RNA significantly increases the mobility of RNase E condensates, regardless of the presence of degradosome clients. Interestingly, the addition of RNase E and PNPase in the absence of RNA showed a recovery $\tau_{1/2}$of 0.38 min. This suggests that even though the degradosome proteins don't dramatically stimulate the rate of condensation, the degradosome protein interactions likely do influence the mobility of RNase E within the droplets, either indirectly through altering the structure of the CTD or directly by influencing the multivalent protein-protein interactions in the condensed state. Altogether, RNA appears to stimulate the rate of RNase E condensation, while the recruitment of RNA or protein clients helps to increase the mobility of RNase E within the condensate which may help promote enhanced biochemical activity.

Discussion

A complex protein interaction network impacts BR-body condensation and composition

BR-body proteomics revealed >100 different proteins of various biochemical functions are enriched, suggesting they are more complex than previously assumed. Importantly, many other scaffolds that can undergo heterotypic phase separation with RNA are also enriched in BR-bodies, which suggests that

many cellular RNP condensates exist and interact with BR-bodies. Five proteins which interact with RNase E were identified as scaffolds that can phase separate with RNA *in vitro*, including RhlE, DeaD, Hfq, FabG, and MetK. Together with RNApol condensates identified previously[5], this suggests that bacteria contain many RNP condensates likely help coordinate multi-step reactions in RNA processing[3]. As observed for yeast P-bodies, a set of "core" proteins were found to be quantitatively enriched[27] and likely homogeneously represented in these structures, were successfully reconstituted *in vitro* with similar dynamics properties and stoichiometries identified[28]. We observed that a subset of BR-body enriched proteins known to stoichiometrically assemble the RNA degradosome (RNase E, RhlB, Aconitase, and PNPase), appear to be uniformly enriched in BR-bodies *in vivo*[4] and selectively recruited to RNase E condensates *in vitro* (Fig 6). This suggests that the RNA degradosome likely composes the "core" set of proteins making up each BR-body. An important goal working forward will be to define the role of BR-body localization to each of the core enzymes involved in the RNA decay process. Indeed, by using a two protein BR-body system using only RNase E and PNPase, PNPase activity was observed to be directly stimulated via condensation with RNase E[17], suggesting organization in BR-bodies may help to stimulate RNA degradosome activity. By testing the full complement of "core" BR-body proteins and also the set of "accessory" BR-body associated proteins, we will likely be able to delineate the normal vs specialized functions of BR-bodies.

As DEAD box RNA helicases appear to be important players in biomolecular condensates[38,42], we observed that RhlE and DeaD act as scaffolds that undergo RNA dependent phase-separation *in vitro*, while RhlB did not, similar to what was observed for their *E. coli* homologues[38], suggesting phase separation is a conserved feature of these proteins. Interestingly, we observed strong recruitment of RhlE and RhlB into RNase E condensates, while DeaD was observed to be recruited to a lower extent (Fig 4). While RhlB foci were dissociated in cells after RNase E depletion and showed strongly correlated localization with RNase E[4], RhlE remained localized in foci even after RNase E depletion and showed heterogenous partially overlapping localization with RNase E (Fig 2). Taken together, this suggests all BR-bodies likely contain RhlB, a core part of the RNA degradosome, while the heterogeneity of RhlE colocalization suggests that some BR-bodies lack this protein. The function of DEAD box proteins in BR-bodies is not well understood, however, RhlE becomes more highly expressed when *C. crescentus* is grown in the cold[40] which may alter the composition and function of BR-bodies in these conditions.

As the BR-body transcriptome previously revealed that poorly translated mRNAs and small RNAs were highly enriched substrates, the BR-body proteomics identified Hfq as a BR-body enriched protein. Interestingly, the protein Hfq which is known to chaperone small RNAs to base-pair to their target mRNAs and repress translation/induce decay[43–47], was found to be enriched in BR-bodies, to form foci in *C. crescentus*, and to phase separate with RNA *in vitro*. *E. coli* Hfq was recently found to phase separate with DNA ,polyphosphate[39], and RNA[10], and its condensation is promoted *in vitro* by its intrinsically disordered CTD[39]. Interestingly, *E. coli* Hfq foci were previously identified to colocalize with RNase E in Nitrogen starved *E. coli* cells[7], and while Hfq is not a core member of the *E. coli* or *C. crescentus* RNA degradosome, it has been found to associate with RNase E in multiple species[48]. Interestingly, we observed that *C. crescentus* Hfq is readily recruited into RNase E-RNA condensates, but RNase E was not recruited into Hfq-RNA condensates, suggesting directionality in forming a mixed condensate. *E. coli* Hfq condensates were found to promote sRNA-mRNA annealing[10] and RNase E IDR mutants that prevent BR-body phase separation were found to prevent sRNA-mRNA silencing[49]. Therefore the coordination of

Hfq with BR-bodies likely helps to degrade translationally repressed mRNAs as has been proposed for miRNA/siRNA/lsm enrichment in P-bodies[22].

The identification of BR-body associated proteins which can dissolve BR-bodies (ribosomal protein S1 and MetK) suggests they may play important regulatory roles in controlling BR-body assembly. Ribosomal protein S1 appears to dissolve RNase E condensates via its RNA binding capacity, while MetK appears to dissolve RNase E via protein-protein interaction with RNase E (Fig 5). Ribosomal protein S1 is present in a ribosome bound and a ribosome free form where it is known to unfolds structured mRNAs in preparation for translation initiation[50], and protect mRNAs from RNase E dependent decay[51]. Since BR-bodies and ribosomes compete for mRNA substrates[4], ribosomal protein S1 may prevent BR-body condensation on highly translated mRNAs by locally disrupting RNase E condensation when in polysomes. Alternatively, if ribosomal protein S1 dissociates from the ribosome, it may be able to globally dissolve BR-bodies, potentially acting as a sensor of translation. MetK an essential enzyme in which generates S-adenosyl-methionine and which we identified could assemble RNP condensates. While it was identified as an RNase E binding protein from CoIP in cells grown in the cold, we identified a weak *in vitro* CoIP of RNase E and MetK proteins (Fig 5), suggesting MetK likely inhibits RNase E condensation directly from blocking multivalent interactions, or indirectly by altering the conformation of RNase E. Despite its rather weak RNA binding observed *in vitro*, MetK from *C. crescentus* phase separated in the presence of RNA, and homologs from *S. meliloti* and *E. coli* were identified to bind RNA[52]. Since MetK is the sole enzyme creating SAM in *C. crescentus*, perhaps it might act as a metabolic sensor that could tune the number of BR-bodies to Carbon availability. In line with this hypothesis, its levels are dramatically altered upon Carbon starvation[53].

Critical importance of RNA in bacterial RNP body condensation

Excitingly, reconstitution of minimal BR-body cores revealed that RNA, which was hypothesized to play a key role in BR-body assembly *in vivo*[4], also plays a key role in BR-body assembly *in vitro*. We observed that RNA can kinetically stimulate the rate of BR-body condensation on the sub-minutes timescale (Fig 7), further suggesting rifampicin-induced RNA depletion is likely the main cause of RNase E's robust foci dissolution and not other cellular perturbations from this drug (such as nucleoid expansion[54]). The addition of RNA degradosome proteins does not alter the rate of RNase E condensation, however, does appear to enhance RNase E mobility by FRAP (Fig 7). Based on BR-body transcriptomics, these structures are mostly enriched for long poorly translated mRNAs and small RNAs and depleted of rRNA and other highly structured ncRNAs[29]. This suggests that at least under logarithmic growth conditions, availability of poorly translated RNA helps catalyze rapid BR-body assembly. Interestingly, BR-bodies could be induced with some client proteins in the absence of RNA, such as PNPase, however, the rate of the condensation was far slower than in the presence of RNA. While likely not relevant under log phase growth conditions as BR-bodies were observed to have sub-minutes dynamics[4], such assemblies might occur under non-growing conditions, like stationary phase.

The identification of five new RNP condensates associated with BR-bodies suggests these structures likely have a broader role in bacterial cell organization than previously anticipated. Indeed, recent high-throughput methods designed to detect proteins crosslinked to RNA identified >1100 RNA binding proteins in *E. coli* including many metabolic enzymes[55,56]. Indeed, we identified two metabolic enzymes, MetK and FabG, which have the capacity to phase separate with RNA (Fig 3). While the ability of metabolic enzymes to bind to RNA is referred to as "moonlighting" RNA binding activity[57], it's possible

that due to large number of RNA binders RNP condensates plays a broad role in organizing metabolic pathways in the bacterial cytoplasm. While experimentation to identify and characterize new condensates is slow, bioinformatic prediction of proteins that can undergo phase separation is making progress, however, even next generation algorithms do not accurately predict the phase separation of all five of these proteins. Perhaps current phase separation prediction algorithms rely too much on IDR predictions, which appear to often affect phase separation, but are not always required[58]. In developing next generation algorithms to predict phase separation, it will be important for the training data sets to include bacterial phase separating proteins so we can begin to make accurate estimates for the fraction of the bacterial proteome that is able to phase separate.

Materials and Methods

Caulobacter crescentus cell growth

All *C. crescentus* strains used in this study were derived from the wild-type strain NA1000[59], and were grown at 28˚C in peptone-yeast extract (PYE) medium or M2 minimal medium supplemented with 0.2% D-glucose (M2G)[60]. When appropriate, the indicated concentration of vanillate (500 mM), xylose (0.2%), gentamycin (Gent) (0.5 mg/mL), kanamycin (Kan) (5 mg/mL), spectinomycin (Spec) (25 mg/mL), and/or streptomycin (Strp) (5 mg/mL) was added. Strains were analyzed at mid-exponential phase of growth (OD 0.3-0.6). Optical density was measured at 600 nm in a cuvette using a Nanodrop 2000C spectrophotometer.

BR-body enrichment assay and LC-MS proteomics

BR-body enrichment was performed as in[30]. Enriched BR-bodies were then resuspended in buffered SDS before proteomics sample preparation.

Suspension Trapping (S-Trap) Sample Preparation:

100 µg protein lysate (JS221 or JS299) was prepared in triplicate according to the manufacturer's instructions. Trypsin was resuspended in a 50 mM ABC buffer and added to S-Traps at a 1:50 (enzyme:protein w/w) ratio and incubated for 8 hours at 37˚C. After the digestion, peptides were eluted according to the manufacturer's protocol and vacuum centrifuged to dryness prior to desalting.

Solid Phase Extraction (SPE):

All samples were desalted prior to MS analysis with 10mg HLB cartridges according to manufacturer's instructions as in [61]. Samples were dried prior to analysis and stored at -80˚C until re-suspension for LC-MS/MS.

Analysis via nano UHPLC-MS/MS:

Dried digests were resuspended in 0.1% formic acid in water to a concentration of 250 ng/µL. 2 µL of solution was injected onto a 100mm x 100µm C_{18} BEH reverse phase chromatography column with an autosampler (nanoACQUITY, Waters Corporation). Peptides were separated over a 95 minute segmented gradient from 4-35% B (A= H_2O + 0.1% FA, B=acetonitrile + 0.1% FA) MS-MS/MS was performed on a Q-Exactive HF mass spectrometer via electrospray ionization (Thermo Fisher Scientific). Samples were collected in biological triplicate, and data was acquired in technical triplicate injections using a TOP17 data-dependent method (DDA).

Peptide-Spectrum Matching (PSM):

RAW files from technical and biological triplicates were processed for peptide identification, protein inference, and false-discovery rate using the MetaMorpheus search engine[62]. A *C. crescentus* FASTA from UniProt (proteome ID UP000001364) was used with a common contaminant file. Data were first calibrated prior to search ('Traditional') using the default parameters. For 'Main' search, additional parameters included a maximum of two missed cleavages, two variable modifications per peptide, and a minimum peptide length of seven amino acids. The precursor mass tolerance was set to 5 ppm and the product mass tolerance was set to 20 ppm. The 'common' fixed and 'common' variable modifications were selected, and identifications were filtered to a q-value of <0.01. RAW data files are available through MassIVE with accession number (MSV000090894).

In vivo localization of BR-body associated proteins

All *C. crescentus* protein fusion strains were grown in PYE-Kan or PYE-Gent media overnight. The next day, from the log-phase cultures, a few dilutions were done in M2G media containing appropriate amount of Kan or Gent and grown for overnight. The next day, the mid log-phase cultures were induced with 500 mM vanillate and grown for 6 hours. 1µL of the cells were spotted on a M2G 1.5% agarose pad and imaged using a YFP filter cube.

RNase E depletion

Depletion strains containing the xylose inducible copy of RNase E were first grown overnight in M2G-Kan-Gent media containing 0.2% xylose. The next day, from the log-phase cultures, a few dilutions were done in M2G-Kan-Gent media containing 0.2% xylose overnight. Mid-log phase cells were then washed 3 times with 1 mL growth media and resuspended in growth media and split into two tubes and one treated with 0.2% xylose. Depletion strains were analyzed at mid-exponential phase of growth (OD 0.3-0.6) and after 24 hours of depletion of xylose. 1 µL of the cells under each condition was spotted on a M2G 1.5% agarose pad and imaged using a YFP filter cube.

Colocalization of YFP tagged proteins with BR-body marker Aconitase-mCherry

Dual-labeled strains expressing YFP tagged proteins with BR-body marker Aconitase-mCherry were first grown overnight in PYE-Kan-Spec-Strp media in 3 dilutions. Mid log-phase cells were split into two tubes, and one was treated with 0.02% xylose and grown for 3.5 hours. 1 µL of the cells under each condition was spotted on a M2G 1.5% agarose pad and imaged using YFP and TX-Red filter cubes. Fluorescence level analysis of the droplets was performed using MicrobeJ[63]. The correlation analysis was performed in Microsoft Excel.

Dissolution of MetK and ribosomal protein S1

Strains expressing MetK and ribosomal protein S1 with BR-body marker Aconitase-mCherry were first grown overnight in PYE-Kan-Spec-Strp media in 3 dilutions. Mid log-phase cells were split into two tubes, and one was treated with 0.2% xylose and grown for 6 hours. 1 µL of the cells under each condition was spotted on a M2G 1.5% agarose pad and imaged using TX-Red filter cubes.

Cell imaging

Around 1 µL of cells were immobilized on 1.5% agarose pads made with M2G medium on microscope slides (Thermo SCIENTIFIC 3051), air dried and imaged with immersion oil on a coverslip. All images were collected using a Nikon Eclipse NI-E with CoolSNAP MYO-CCD camera and 100x Oil CFI Plan Fluor (Nikon) objective, driven by Nikon elements software. The filter sets used for YFP, CFP and mCherry imaging were chroma 96363, 96361, and 96322 models respectively. Cell image analysis was performed using Microbe-J[63].

QUANTIFICATION AND STATISTICAL ANALYSIS

Foci quantification

In vivo protein fusion foci were quantified using Microbe J[63]. Cell outlines were first identified using the medial axis algorithm in the phase channel with minimal cell length of 1.35 µm and the segmentation option. Cell outlines were then manually curated to remove cells containing erroneous outlines. Next, the maxima function was used with ''foci'' option with minimal area of 0.01 μm^2 and minimal length of 0.1 µm with the segmentation option on and the association inside option on. Tolerance and Z-score parameters tuned for each protein fusion type.

To quantify the average foci per cell of each strain, three replicates were performed in three different days and 3 images were analyzed from each day. We summed all foci identified in each cell, divided by the total of the cell to calculate number of foci per cell.

RNA extraction

For RNA extraction mid-log phase cells (0.3 to 0.5 OD600) were pelleted at 20,000 g for 10 minutes in a microcentrifuge. Then, cells were resuspended in 1mL 65˚C Trizol (1mL for each 1 mL of NA1000 cell) and incubated at 65˚C for 10 min in a heat block. 200mL of chloroform was added and incubated for 5 min at room temperature. The samples were then spun at max speed (20,000 g) in a microcentrifuge for 10 min at room temperature. The aqueous layer was removed and RNA samples were precipitated using 700 mL isopropanol at -80˚C for 1 hour and spun at 20,000 g for 1 hour at 4˚C. The supernatant was removed and the pellet was washed with 1 mL of 70% ethanol. The samples were then spun again for 10 min at 20,000 g at 4˚C, the supernatant was removed, and the pellet was resuspended in RNase-free water. RNA samples were run on 1X TBE/7M Urea denaturing PAGE gels and visualized with SYBR-Gold nucleic acid gel stain.

Protein purifications:

The protein coding genes were cloned into pET His6 MBP TEV or pET His6 G TEV or pET28a plasmids and the expressed proteins are purified by His tag affinity purification followed by the removal of MBP or G tag by TEV proteolysis. RNase E CTD, RhlB, RhlE -IDR were expressed as N-terminal MBP fusions, all the other proteins were expressed as N-terminal G protein fusions. Briefly, the proteins are expressed in BL21 DE3 cells by inducing with 0.5mM IPTG at 37° C for 3.5 hours in 2X Luria-Bertani media, and the cells pelleted at 5000 rpm for 20 minutes were lysed in a lysis buffer (20mM Tris pH 7.4, 500mM NaCl, 10% Glycerol, 10mM Imidazole, 1mM PMSF, 1 tablet protease inhibitor cocktail and DNase I) at 4° C using a sonicator with 10 seconds pulse on and 30 seconds pulse off times for 18 cycles. The lysed cells were centrifuged at 15000 rpm for 45 minutes and the resultant supernatant was loaded onto equilibrated Ni-NTA resin, the protein bound resin was washed with 10 column volumes each of lysis

buffer, chaperone buffer (20 mM Tris pH 7.4, 1 M NaCl, 10% Glycerol, 10 mM Imidazole, 5 mM KCl, 10 mM MgCl2, 2 mM ATP) and low salt buffer (20 mM Tris pH 7.4, 1 M NaCl, 10% Glycerol, 10 mM Imidazole) respectively. The proteins were eluted in elution buffer (20 mM Tris pH 7.4, 150 mM NaCl, 10% Glycerol, 250 mM Imidazole) and dialyzed into storage buffer (20 mM Tris pH 7.4, 150 mM NaCl). The contaminant proteins were removed by passing through S200 size exclusion column. The concentrated proteins were stored in -80° C freezer.

RNase E CTD purification: His6-MBP-TEV-RNase E CTD was expressed and purified in the same way as described above except the lysis buffer additionally contained 1M NaCl and 0.1% Triton X-100.

Hfq purification: Hfq protein was expressed at 18° C for 16 hours. Lysis buffer and elution buffer contained 1 M NaCl instead of 150 mM and 500 mM NaCl respectively. To remove the contaminating nucleic acids, the His tag affinity purified protein was treated with 30 µg/mL RNase A and 5 U/mL DNase I for 1 hour at 37° C, concentrated and loaded onto HiLoad 16/60 Superdex 200 size exclusion column (GE healthcare). The absence of RNase A was further validated by incubating RNA with the protein.

Protein labeling:

Cyanine 5 NHS ester labeling of proteins:

Labeling reactions were carried out according to manufacturer's protocol (Lumiprobe). Cy5 NHS ester dye dissolved in DMSO was incubated with proteins at an equal ratio in 0.1M sodium bicarbonate buffer pH 8.5 at room temperature for 4 hours. Protein labeling calculator https://www.lumiprobe.com/calc/protein-labeling was used to calculate the amount of protein and dye used in the labeling reactions. The excess of dye was removed by dialyzing against protein storage buffer (20mM Tris pH 7.4, 150mM NaCl) using a 3 kDa cut off dialysis cassette. Degree of labeling was calculated using the formula:

$$number\ of\ cy5\ dye\ per\ protein = \frac{molarity\ of\ cy5\ dye}{molarity\ of\ protein}$$

$$[molarity\ of\ cy5\ dye] = \frac{A650}{\mathrm{\mathfrak{E}}650}$$

$$molarity\ of\ protein = \frac{A280c}{\mathrm{\mathfrak{E}}280}$$

$$A650 = conjugate\ absorbance\ at\ 650nm$$

$$\mathrm{\mathfrak{E}}650 = molar\ extinction\ coefficient\ of\ Cy5\ dye$$

$$A280c = conjugate\ corrected\ absorbance\ at\ 280nm = A280 - \big(A650 * (0.05)\big)$$

$$\mathrm{\mathfrak{E}}280 = molar\ extinction\ coefficient\ of\ protein$$

***In vitro* phase separation experiments and droplet assays**

Proteins at their *in vivo* concentrations are incubated in the presence or absence of *C. crescentus* total RNA (20 ng/µL) in 20mM Tris pH 7.4, 100mM NaCl for 30 minutes at room temperature. The mixture was pipetted onto glass slide, covered with a cover slip, and imaged using Nikon epifluorescence

microscope. For quantification of number and distribution of droplets, 10 images for each protein were analyzed using 'analyze particles' function in Image J. See table 1 for detailed protocol.

For recruitment assays, 6 µM RNAse E CTD was incubated with 20 ng/ µL of *C. crescentus* total RNA in 20mM Tris pH 7.4, 100mM NaCl for 20 minutes at room temperature, followed by the addition of Cy5 labeled client proteins and additional incubation for 20 minutes before imaging. The level of recruitment was assessed by calculating the partition coefficient of client proteins. 30 droplets were analyzed in each case.

$$partition\ coefficient = \frac{mean\ fluorescence\ intensity\ inside\ the\ droplets}{mean\ fluorescence\ intensity\ outside\ the\ droplets}$$

ImageJ software was used to quantify the mean fluorescence and the data was plotted in PlotsOfData[64]. Coassembly experiments were performed by mixing all the components and incubated for 30 mins at room temperature before imaging.

For salt and RNA dependency experiments, preformed protein and RNA condensates were incubated with either varying concentrations of NaCl or RNase A for 30 minutes at room temperature before imaging the solution on a glass slide using phase contrast microscope.

RNase E condensation induction in the absence of RNA was carried out by adding client proteins at varied concentrations to 6 µM RNase E CTD in 20mM Tris, 100mM NaCl and incubated for 30 minutes at room temperature. The solution was imaged on a glass slide using phase contrast microscope.

In-vitro protein pull down assay

RNAse E CTD tagged with Maltose Binding Protein (MBP) or MBP only was incubated with bait proteins in pull down binding buffer (20mM Hepes pH 7.4, 100mM NaCl, 2% Glycerol, 2mM DTT) for 60 mins at room temperature. 100 µL of Dextrin Agarose resin was added to the above mixture and incubated for another 90 minutes at 4°C on a tube rotator. The samples were washed four times with 1 mL of wash buffer (20mM Hepes pH 7.4, 100mM NaCl) each time. Bound proteins were eluted with 100 µL of elution buffer (20mM Hepes pH 7.4, 150mM NaCl, 10mM Maltose) at 30ºC with constant shaking. The eluted proteins were resolved on SDS PAGE gel.

Electrophoretic mobility shift assay

RNA (50 nM) was incubated with specified concentrations of proteins for 30 mins at room temperature in binding buffer consisting of 20mM Tris pH 7.4, 150mM NaCl, 5% Glycerol, 2mM DTT, 1mM EDTA, 10 µg/mL BSA. The incubated samples were resolved on a 5% Acrylamide/Bis-acrylamide native gel (prepared in TBE buffer) at 4ºC in 0.5X TBE running buffer. The gel was stained with SYBR GOLD for 20mins and scanned using a Typhoon scanner for RNA/RNA-protein complexes detection.

Determination of order of assembly of RhIE, RNase E and Aconitase foci

C. crescentus JS716 (RhIE-YFP/Aconitase-mCherry) and JS452 (RNase E-YFP/Aconitase-mCherry) were grown overnight in PYE medium containing kanamycin (5 µg/mL), spectomycin (25 µg/mL) and streptomycin (5 µg/mL) until the cultures reached mid log-phase (OD~0.3). Prior to imaging, the cells were diluted to 0.05 OD in PYE media and induced with 0.02% xylose for 15 minutes at 28 °C. Aliquots of 1.5 µL of culture were spotted onto pads of 2% agarose in M2G medium and sandwiched between two

coverslips. Cells were imaged with an Olympus IX71 inverted epifluorescence microscope with a 100× objective (NA 1.40, oil immersion) kept at 28 °C using at objective heater (Bioptechs). The YFP fusion proteins were imaged under excitation from a 488-nm laser (Coherent Cube 488-50; 0.4 W cm^{-2}) and the mCherry fusions were imaged under excitation from a 561-nm laser (Coherent Sapphire 561-50; 2.0 W cm^{-2}). Both channels were imaged simultaneously on a 512 × 512 pixel Photometric Evolve electron-multiplying charge-coupled device (EMCCD) camera, using an OptoSplit II image splitter (Cairn Research) with a 635-nm long pass filter and a 525/50 nm bandpass filter. An integration time of 250 ms with a delay between frames of 5 s was used, where a shutter blocked irradiation during the delay time to minimize photobleaching of YFP and mCherry.

To analyze the fluorescence intensities, the mean intensity of each cell in each channel was first subtracted from the movies. Foci were then detected by eye in the background-subtracted movies, and the mean and maximum intensities within the 9 × 9 pixel region of interest (ROI) surrounding each focus was measured in both channels. Time zero was set to be the frame immediately preceding the first frame with an ROI mean intensity at least 10% higher than the maximum intensity value in the ROI in the previous frame. This time zero was also assigned as time zero on the other channel. Subsequently, the maximum intensity within the ROIs were divided by the maximum intensity of the ROI in the time zero frame to determine the fluorescence intensity enhancement of each focus at each time.

Condensate growth kinetic assays

Time lapse images were acquired using Zeiss LSM 800 microscope. 6 µM of RNase E CTD YFP (RCY) was spotted onto a glass slide, and either the RNA or proteins or both at specified concentrations was pipetted onto RCY solution. The image acquisition was started before the addition of RNA or proteins or both, but the zero-minute time point was calculated from the time they are added to RCY solution on glass slide. The zero-minute time point for 'RCY only' started from the time the sample was spotted onto glass slide. The images were acquired for 2.5 minutes with 50 ms time interval. The data was quantified in Image J and plotted in MS Excel.

FRAP assays

FRAP was performed according to a standard protocol (Jing et al., 2018). Briefly, the measured F(t) over the bleached circular area of d = 2 µm in diameter, normalized by that of the unbleached region of the same diameter, F(0), was fitted by a one-phase exponential function using the "Bottom to (SpaZeisn + Bottom)" analysis as $F(t)/F(0) = Bottom + Span*(1 - \exp(-t \ln 2/\tau_{1/2}))$, where $\tau_{1/2}$ is the halftime for diffusion. The apparent diffusion coefficient, D, of f-dextran in PSBMA–{W12} coacervates was obtained from $\tau_{1/2}$ according to $D = d2/(4\tau_{1/2})$.

Figure Legends

Figure 1. BR-body enrichment proteomics identifies BR-body associated proteins. A) *Caulobacter crescentus* BR-body enrichment[30] was performed, followed by LC-MS/MS proteomics to identify BR-body associated proteins. JS299 (an RNase E active site mutant) was used to isolate BR-bodies, and JS221 (an RNase E mutant lacking the C-terminal disordered region that cannot form BR-bodies) was used as a negative control. B) BR-body enrichment analysis from the LC-MS/MS proteomics data. The RNA degradosome proteins were identified by pulldown from[31,34,40]. Polar proteins were identified as interactors with PopZ[65] or polar condensates with interactions with PopZ, PodJ, or SpmX. Polar proteins

measured in the negative control but undetected in the BR-body enriched samples were plotted at <-5. T-tests with uneven variance were used for statistical comparison. GO-term enrichment for localization and protein function were performed using NCBI DAVID[66]. C) Localization pattern of foci-forming YFP fusions. All genes were placed under control of the vanillate promoter grown in M2G minimal media. *In vivo* protein fusion strains were analyzed at mid-exponential phase of growth (OD 0.3-0.6) following 6-hours of induction with 0.5mM vanillate and quantified using Microbe J[63]. Three replicates were performed in three different days and 3 images were analyzed from each day to calculate the average number of foci/cell. A minimum of 150 cells were used for the analysis. Error bars represent standard error. Raw images in supplementary figure 1(Fig S1).

Figure 2. RNase E is required for foci localization of most BR-body associated proteins. A) Subcellular localization patterns of *C. crescentus* protein-YFP strains expressed from the *vanA* locus in the RNase E depletion background where the sole copy of the RNase E gene is controlled by the xylose promoter. The YFP intensity of aconitase-YFP was too low to measure when expressed from the vanillate promoter, so a native gene fusion was used instead. YFP intensity of each image was normalized from its brightest level relative to its background level. Depletion strains were analyzed at mid-exponential phase of growth (OD 0.3-0.6) and after 24 hours of depletion of xylose. B) Quantitation of the number of *Ccr* protein-YFP foci per cell measured in M2G minimal media with xylose (+Xyl) and M2G minimal media lacking xylose (-Xyl) for the same strains in panel A. All images were quantified using Microbe-J[63]. Three replicates were performed in three different days and 3 images were analyzed from each day to calculate the average # foci/cell. A minimum of 175 cells were used for the analysis. Error bars represent standard error. Observed dependence on RNase E is indicated on the right.

Figure 3. Some BR-body enriched proteins can drive RNA dependent biomolecular condensation. A) (Left) Domain organization of proteins that undergo LLPS. The red line indicates disordered region as predicted by PONDR. (Right) Disorderness[67], Pscore[62], Catgranule[68] and DeePhase[69] scores to predict the propensity of LLPS B) Phase contrast microscopy images of the purified proteins incubated at their *in vivo* concentrations in standard buffer (20mM Tris pH 7.4, 100mM NaCl, 1mM DTT) in the presence and absence of *C. crescentus* total RNA (30ng/uL). Scale bar is 5 µm. C) Droplets are dissolved by NaCl and RNase A. The dissolution of droplets was tested at different NaCl concentrations (0.1, 0.5 and 1M) and RNase A (1 µg). All the proteins were found to be NaCl and RNase sensitive.

Figure 4. Many BR-body associated proteins are directly recruited to RNase E condensates *in vitro.* A) Cartoon showing the *in vitro* RNase E droplet recruitment assay. Cy5 labeled proteins are added to preformed RNase E CTD+RNA droplets. Microscopy images of the droplets are taken in Phase contrast and Cy5 fluorescence, and the partition coefficients of the fluorescence signal is calculated for each droplet. B) Partition coefficient (PC) of Cy5 labeled client proteins in RNase E CTD droplets. Negative controls BSA Cy5 and SpmX Cy5 have partition coefficients of 1. The black horizontal line through the plot indicates a PC of 1 which indicates the no enrichment baseline. PC of ribosomal protein S1 and MetK proteins could not be determined because of the dissolution of droplets. The data was quantified in imageJ software and plotted in PlotsofData[64]. For the example images presented, left image is phase contrast and the right image is Cy5 channel of each indicated protein. Scale is 10 µm for all images.

Figure 5. Ribosomal protein S1 and MetK dissolve BR-bodies *in vitro* and *in vivo.* A) Microscopy images of *in vitro* RNase E droplets incubated with either ribosomal protein S1 or MetK. RNA induced RNase E droplets are shown on the top, while PNPase induced RNase E droplets are shown below. Scale is 10 µm

for all images. Below is a proposed cartoon of the RNA dependence of dissolution of each protein. B) RNA and protein binding data for ribosomal protein S1 and MetK with 1 µM RNA. RNA was visualized by sybr gold staining. C) RNase E coIPs with Acontiase and MetK. Co-IP of mbp-RNase using 1 µM RNase E incubated with 5 µM of the indicated proteins. Eluates were run on SDS-PAGE and stained with simply blue safestain (thermofisher). MBP mock reactions were used as a negative control. D) BR-bodies (marked with aconitase-mCherry) are dissolved upon overexpression of ribosomal protein S1 or MetK from the pBX multicopy plasmid. Quantitation of the average Aconitase-mChy foci/cell was performed using Microbe-J and is plotted on the right (error bars represent standard error). A minimum of 700 cells were used for the analysis.

Figure 6. BR-body associated drivers have distinct condensation and client recruitment profiles. A) Scaffold proteins recruit a distinct subset of client proteins. Each RNA degradosome client labeled with Cy5 was tested for recruitment into each BR-body associated scaffold. Each dot in (A) and (B) plots indicate the partition coefficient in a single droplet. Partition coefficient was calculated from at least 50 droplets in each case. The data was quantified in imageJ and plotted in PlotsofData. B) BR-body associated scaffolds drive a complex network of dependencies controlling phase separation. Each protein scaffold was incubated with RNA and allowed to phase separate. Then a small concentration of Cy5 labeled proteins were tested for entry into the condensate by measuring the partition coefficients of the Cy5 channel. C) Order of assembly experiments using GFP-RNase E and RhlE-Cy5 condensates. Condensed simultaneously indicates that both proteins were added together before the addition of RNA to trigger condensation, “condensed separately” indicates that both proteins were incubated with RNA yielding separate condensates that were then mixed together. D) Colocalization of YFP tagged proteins with BR-body marker Aconitase-mCherry. Colored arrows indicate the pattern of localization observed for induvial foci. Correlation plot with the correlation value of each channel for many line traces across Aconitase-mCherry Foci. The correlation of YFP and mCherry signal is calculated for each line trace, and each line trace correlation value is plotted as a single dot on the plot. The median value is represented as a black line. Statistics were based upon 2-tailed T-test with unequal variance. E) *In vivo* order of foci assembly. Time-lapse two-color imaging of RhlE-YFP and Aconitase-mCherry proteins was performed, , and the evolution of the intensity of each focus after formation is plotted. (i) Intensity evolution in cells in which both Aconitase-mCherry and RhlE-YFP condensates are formed approximately at the same time. The middle line indicates the average value, and the colored region represents the standard deviation between all replicate events. N is the number of events imaged. (ii) Cells in which RhlE-YFP condensates were formed first and the subsequent appearance of Aconitase-mCherry in RhlE-YFP condensates was tracked. (iii) Cells in which Aconitase-mCherry condensates were formed first and the subsequent appearance of RhlE-YFP in Aconitase-mCherry condensates was tracked.

Figure 7. RNA stimulates rapid BR-body condensation *in vitro*. A) Time lapse imaging of RNase E CTD YFP (RCY) condensate formation. 6 µM RCY assembly was monitored either alone or with different combinations of 100ng/µL RNA, 3 µM PNPase, or all degradosome proteins (3 µM PNPase, 2 µM RhlB, 5 µM RNase D1, and 5 µM Aconitase) as indicated on the left. All the images were captured at 20X magnification at the time points indicated above. The scale bar is 20 µm. B) Quantification of condensate growth by calculation of % area occupied in the time lapse experiments from panel A. The data was quantified in imageJ, averaged from three independent replicates, and plotted in MS Excel. C) Apparent FRAM recovery for droplets with the indicated composition. Since no RCY condensates are

present at 6 µM, the concentration was increased to 30 µM to induce condensates. The values are averages from at least six different droplets, and error bars represent the standard deviation.

Graphical Abstract. Summary of BR-body protein interactome. Scaffolds/Drivers of phase separation are drawn as blue circles, Protein inhibitors of phase separation are drawn in red circles, and clients of BR-bodies are drawn in green circles. Lines between two protein circles represent a direct interaction.

Authors Contribution:

VN performed protein purifications, all *in vitro* experiments, and *in vivo* experiments. IWR performed protein purifications, *in vivo* experiments (*in vivo* expression experiments, *in vivo* depletion experiments, and colocalization experiments), and made plasmids and strains for *in vivo* experiments. VN, AH, JV performed droplet kinetic assays and FRAP experiments. KM, AG, and YH purified proteins. NM purified BR bodies for BR-body proteomics. CBM and MC performed LC-MS data collection and analysis. LAOR performed RhlE *in vivo* assemble experiments.

Acknowledgements:

NIH grant R35GM124733 to JS. NIH grants R01GM143182 and R01GM144731 to JB. NIH Grant R01GM136863 to WSC. NSF grant CMMI-1914436 to YZ. NIH grant R01GM139277 to MC. We would like to acknowledge the Mass Spectrometry and Proteomics Facility at Notre Dame.

References:

1. Azaldegui, C.A., Vecchiarelli, A.G., and Biteen, J.S. (2021). The emergence of phase separation as an organizing principle in bacteria. Biophysical Journal *120*, 1123–1138. 10.1016/j.bpj.2020.09.023.

2. Banani, S.F., Lee, H.O., Hyman, A.A., and Rosen, M.K. (2017). Biomolecular condensates: organizers of cellular biochemistry. Nature Reviews Molecular Cell Biology *18*, 285–298. 10.1038/nrm.2017.7.

3. Nandana, V., and Schrader, J.M. (2021). Roles of liquid–liquid phase separation in bacterial RNA metabolism. Current Opinion in Microbiology *61*, 91–98. 10.1016/j.mib.2021.03.005.

4. Al-Husini, N., Tomares, D.T., Bitar, O., Childers, W.S., and Schrader, J.M. (2018). α-Proteobacterial RNA Degradosomes Assemble Liquid-Liquid Phase-Separated RNP Bodies. Molecular Cell *71*, 1027-1039.e14. 10.1016/j.molcel.2018.08.003.

5. Ladouceur, A.-M., Parmar, B.S., Biedzinski, S., Wall, J., Tope, S.G., Cohn, D., Kim, A., Soubry, N., Reyes-Lamothe, R., and Weber, S.C. (2020). Clusters of bacterial RNA polymerase are biomolecular condensates that assemble through liquid–liquid phase separation. PNAS *117*, 18540–18549. 10.1073/pnas.2005019117.

6. Lasker, K., von Diezmann, L., Zhou, X., Ahrens, D.G., Mann, T.H., Moerner, W.E., and Shapiro, L. (2020). Selective sequestration of signalling proteins in a membraneless organelle reinforces the spatial regulation of asymmetry in Caulobacter crescentus. Nature Microbiology *5*, 418–429. 10.1038/s41564-019-0647-7.

7. McQuail, J., Switzer, A., Burchell, L., and Wigneshweraraj, S. (2020). The RNA-binding protein Hfq assembles into foci-like structures in nitrogen starved Escherichia coli. Journal of Biological Chemistry *295*, 12355–12367. 10.1074/jbc.RA120.014107.

8. Monterroso, B., Zorrilla, S., Sobrinos-Sanguino, M., Robles-Ramos, M.A., López-Álvarez, M., Margolin, W., Keating, C.D., and Rivas, G. (2019). Bacterial FtsZ protein forms phase-separated condensates with its nucleoid-associated inhibitor SlmA. EMBO reports *20*, e45946. 10.15252/embr.201845946.

9. Wang, H., Yan, X., Aigner, H., Bracher, A., Nguyen, N.D., Hee, W.Y., Long, B.M., Price, G.D., Hartl, F.U., and Hayer-Hartl, M. (2019). Rubisco condensate formation by CcmM in β-carboxysome biogenesis. Nature *566*, 131–135. 10.1038/s41586-019-0880-5.

10. Goldberger, O., Szoke, T., Nussbaum-Shochat, A., and Amster-Choder, O. (2022). Heterotypic phase separation of Hfq is linked to its roles as an RNA chaperone. Cell Reports *41*, 111881. 10.1016/j.celrep.2022.111881.

11. Feng, Z., Chen, X., Wu, X., and Zhang, M. (2019). Formation of biological condensates via phase separation: Characteristics, analytical methods, and physiological implications. Journal of Biological Chemistry *294*, 14823–14835. 10.1074/jbc.REV119.007895.

12. Mittag, T., and Pappu, R.V. (2022). A conceptual framework for understanding phase separation and addressing open questions and challenges. Molecular Cell *82*, 2201–2214. 10.1016/j.molcel.2022.05.018.

13. Kar, M., Dar, F., Welsh, T.J., Vogel, L.T., Kühnemuth, R., Majumdar, A., Krainer, G., Franzmann, T.M., Alberti, S., Seidel, C.A.M., et al. (2022). Phase-separating RNA-binding proteins form heterogeneous distributions of clusters in subsaturated solutions. Proceedings of the National Academy of Sciences *119*, e2202222119. 10.1073/pnas.2202222119.

14. Ditlev, J.A., Case, L.B., and Rosen, M.K. (2018). Who's In and Who's Out—Compositional Control of Biomolecular Condensates. Journal of Molecular Biology *430*, 4666–4684. 10.1016/j.jmb.2018.08.003.

15. Hubatsch, L., Jawerth, L.M., Love, C., Bauermann, J., Tang, T.D., Bo, S., Hyman, A.A., and Weber, C.A. (2021). Quantitative theory for the diffusive dynamics of liquid condensates. eLife *10*, e68620. 10.7554/eLife.68620.

16. Taylor, N.O., Wei, M.-T., Stone, H.A., and Brangwynne, C.P. (2019). Quantifying Dynamics in Phase-Separated Condensates Using Fluorescence Recovery after Photobleaching. Biophysical Journal *117*, 1285–1300. 10.1016/j.bpj.2019.08.030.

17. Collins, M., Tomares, D.T., Schrader, J.M., and Childers, W.S. (2022). RNase E biomolecular condensates stimulate PNPase activity. 2022.06.06.495039. 10.1101/2022.06.06.495039.

18. Peeples, W., and Rosen, M.K. (2021). Mechanistic dissection of increased enzymatic rate in a phase-separated compartment. Nat Chem Biol *17*, 693–702. 10.1038/s41589-021-00801-x.

19. Tibble, R.W., Depaix, A., Kowalska, J., Jemielity, J., and Gross, J.D. (2021). Biomolecular condensates amplify mRNA decapping by biasing enzyme conformation. Nat Chem Biol *17*, 615–623. 10.1038/s41589-021-00774-x.

20. Moon, S.L., Morisaki, T., Khong, A., Lyon, K., Parker, R., and Stasevich, T.J. (2019). Multicolour single-molecule tracking of mRNA interactions with RNP granules. Nat Cell Biol *21*, 162–168. 10.1038/s41556-018-0263-4.

21. Pitchiaya, S., Mourao, M.D.A., Jalihal, A.P., Xiao, L., Jiang, X., Chinnaiyan, A.M., Schnell, S., and Walter, N.G. (2019). Dynamic Recruitment of Single RNAs to Processing Bodies Depends on RNA Functionality. Molecular Cell *74*, 521-533.e6. 10.1016/j.molcel.2019.03.001.

22. Hubstenberger, A., Courel, M., Bénard, M., Souquere, S., Ernoult-Lange, M., Chouaib, R., Yi, Z., Morlot, J.-B., Munier, A., Fradet, M., et al. (2017). P-Body Purification Reveals the Condensation of Repressed mRNA Regulons. Molecular Cell *68*, 144-157.e5. 10.1016/j.molcel.2017.09.003.

23. Jain, S., Wheeler, J.R., Walters, R.W., Agrawal, A., Barsic, A., and Parker, R. (2016). ATPase-Modulated Stress Granules Contain a Diverse Proteome and Substructure. Cell *164*, 487–498. 10.1016/j.cell.2015.12.038.

24. Khong, A., Matheny, T., Jain, S., Mitchell, S.F., Wheeler, J.R., and Parker, R. (2017). The Stress Granule Transcriptome Reveals Principles of mRNA Accumulation in Stress Granules. Molecular Cell *68*, 808-820.e5. 10.1016/j.molcel.2017.10.015.

25. Markmiller, S., Soltanieh, S., Server, K.L., Mak, R., Jin, W., Fang, M.Y., Luo, E.-C., Krach, F., Yang, D., Sen, A., et al. (2018). Context-Dependent and Disease-Specific Diversity in Protein Interactions within Stress Granules. Cell *172*, 590-604.e13. 10.1016/j.cell.2017.12.032.

26. Youn, J.-Y., Dunham, W.H., Hong, S.J., Knight, J.D.R., Bashkurov, M., Chen, G.I., Bagci, H., Rathod, B., MacLeod, G., Eng, S.W.M., et al. (2018). High-Density Proximity Mapping Reveals the Subcellular Organization of mRNA-Associated Granules and Bodies. Molecular Cell *69*, 517-532.e11. 10.1016/j.molcel.2017.12.020.

27. Xing, W., Muhlrad, D., Parker, R., and Rosen, M.K. (2020). A quantitative inventory of yeast P body proteins reveals principles of composition and specificity. eLife *9*, e56525. 10.7554/eLife.56525.

28. Currie, S.L., Xing, W., Muhlrad, D., Decker, C.J., Parker, R., and Rosen, M.K. (2022). Quantitative reconstitution of yeast RNA processing bodies. 2022.08.13.503854. 10.1101/2022.08.13.503854.

29. Al-Husini, N., Tomares, D.T., Pfaffenberger, Z.J., Muthunayake, N.S., Samad, M.A., Zuo, T., Bitar, O., Aretakis, J.R., Bharmal, M.-H.M., Gega, A., et al. (2020). BR-Bodies Provide Selectively Permeable Condensates that Stimulate mRNA Decay and Prevent Release of Decay Intermediates. Molecular Cell *78*, 670-682.e8. 10.1016/j.molcel.2020.04.001.

30. Muthunayake, N.S., Al-Husini, N., and Schrader, J.M. (2020). Differential Centrifugation to Enrich Bacterial Ribonucleoprotein Bodies (BR bodies) from Caulobacter crescentus. STAR Protocols *1*, 100205. 10.1016/j.xpro.2020.100205.

31. Hardwick, S.W., Chan, V.S.Y., Broadhurst, R.W., and Luisi, B.F. (2011). An RNA degradosome assembly in Caulobacter crescentus. Nucleic Acids Res *39*, 1449–1459. 10.1093/nar/gkq928.

32. Canestrari, J.G., Lasek-Nesselquist, E., Upadhyay, A., Rofaeil, M., Champion, M.M., Wade, J.T., Derbyshire, K.M., and Gray, T.A. (2020). Polycysteine-encoding leaderless short ORFs function as

842 cysteine-responsive attenuators of operonic gene expression in mycobacteria. Molecular Microbiology
843 *114*, 93–108. 10.1111/mmi.14498.

844 33. Mousseau, C.B., Pierre, C.A., Hu, D.D., and Champion, M.M. (2022). Miniprep assisted
845 proteomics (MAP) for rapid proteomics sample preparation. Anal. Methods, 10.1039.D2AY01549H.
846 10.1039/D2AY01549H.

847 34. Voss, J.E., Luisi, B.F., and Hardwick, S.W. (2014). Molecular recognition of RhlB and RNase D in
848 the Caulobacter crescentus RNA degradosome. Nucleic Acids Research *42*, 13294–13305.
849 10.1093/nar/gku1134.

850 35. Russell, J.H., and Keiler, K.C. (2009). Subcellular localization of a bacterial regulatory RNA.
851 Proceedings of the National Academy of Sciences *106*, 16405–16409. 10.1073/pnas.0904904106.

852 36. Werner, J.N., Chen, E.Y., Guberman, J.M., Zippilli, A.R., Irgon, J.J., and Gitai, Z. (2009).
853 Quantitative genome-scale analysis of protein localization in an asymmetric bacterium. Proceedings of
854 the National Academy of Sciences *106*, 7858–7863. 10.1073/pnas.0901781106.

855 37. Aretakis, J.R., Gega, A., and Schrader, J.M. (2019). Absolute Measurements of mRNA Translation
856 in Caulobacter crescentus Reveal Important Fitness Costs of Vitamin B12 Scavenging. mSystems *4*,
857 e00170-19. 10.1128/mSystems.00170-19.

858 38. Hondele, M., Sachdev, R., Heinrich, S., Wang, J., Vallotton, P., Fontoura, B.M.A., and Weis, K.
859 (2019). DEAD-box ATPases are global regulators of phase-separated organelles. Nature *573*, 144–148.
860 10.1038/s41586-019-1502-y.

861 39. Beaufay, F., Amemiya, H.M., Guan, J., Basalla, J., Meinen, B.A., Chen, Z., Mitra, R., Bardwell,
862 J.C.A., Biteen, J.S., Vecchiarelli, A.G., et al. (2021). Polyphosphate drives bacterial heterochromatin
863 formation. Science Advances *7*, eabk0233. 10.1126/sciadv.abk0233.

864 40. Aguirre, A.A., Vicente, A.M., Hardwick, S.W., Alvelos, D.M., Mazzon, R.R., Luisi, B.F., and
865 Marques, M.V. (2017). Association of the Cold Shock DEAD-Box RNA Helicase RhlE to the RNA
866 Degradosome in Caulobacter crescentus. Journal of Bacteriology *199*, e00135-17. 10.1128/JB.00135-17.

867 41. Thanbichler, M., Iniesta, A.A., and Shapiro, L. (2007). A comprehensive set of plasmids for
868 vanillate- and xylose-inducible gene expression in Caulobacter crescentus. Nucleic Acids Res. *35*, e137.
869 10.1093/nar/gkm818.

870 42. Tauber, D., Tauber, G., Khong, A., Van Treeck, B., Pelletier, J., and Parker, R. (2020). Modulation
871 of RNA Condensation by the DEAD-Box Protein eIF4A. Cell *180*, 411-426.e16. 10.1016/j.cell.2019.12.031.

872 43. Assis, N.G., Ribeiro, R.A., Silva, L.G. da, Vicente, A.M., Hug, I., and Marques, M.V. (2019).
873 Identification of Hfq-binding RNAs in Caulobacter crescentus. RNA Biology *16*, 719–726.
874 10.1080/15476286.2019.1593091.

875 44. Møller, T., Franch, T., Højrup, P., Keene, D.R., Bächinger, H.P., Brennan, R.G., and Valentin-
876 Hansen, P. (2002). Hfq: A Bacterial Sm-like Protein that Mediates RNA-RNA Interaction. Molecular Cell *9*,
877 23–30. 10.1016/S1097-2765(01)00436-1.

878 45. Updegrove, T.B., Zhang, A., and Storz, G. (2016). Hfq: the flexible RNA matchmaker. Curr Opin
879 Microbiol *30*, 133–138. 10.1016/j.mib.2016.02.003.

880 46. Urban, J.H., and Vogel, J. (2008). Two Seemingly Homologous Noncoding RNAs Act Hierarchically
881 to Activate glmS mRNA Translation. PLOS Biology *6*, e64. 10.1371/journal.pbio.0060064.

882 47. Vogel, J., and Luisi, B.F. (2011). Hfq and its constellation of RNA. Nat Rev Microbiol *9*, 578–589.
883 10.1038/nrmicro2615.

884 48. Ikeda, Y., Yagi, M., Morita, T., and Aiba, H. (2011). Hfq binding at RhlB-recognition region of
885 RNase E is crucial for the rapid degradation of target mRNAs mediated by sRNAs in Escherichia coli.
886 Molecular Microbiology *79*, 419–432. 10.1111/j.1365-2958.2010.07454.x.

887 49. Fei, J., Singh, D., Zhang, Q., Park, S., Balasubramanian, D., Golding, I., Vanderpool, C.K., and Ha,
888 T. (2015). Determination of in vivo target search kinetics of regulatory noncoding RNA. Science *347*,
889 1371–1374. 10.1126/science.1258849.

890 50. Duval, M., Korepanov, A., Fuchsbauer, O., Fechter, P., Haller, A., Fabbretti, A., Choulier, L.,
891 Micura, R., Klaholz, B.P., Romby, P., et al. (2013). Escherichia coli Ribosomal Protein S1 Unfolds
892 Structured mRNAs Onto the Ribosome for Active Translation Initiation. PLOS Biology *11*, e1001731.
893 10.1371/journal.pbio.1001731.

894 51. Delvillani, F., Papiani, G., Dehò, G., and Briani, F. (2011). S1 ribosomal protein and the interplay
895 between translation and mRNA decay. Nucleic Acids Res *39*, 7702–7715. 10.1093/nar/gkr417.

896 52. Robledo, M., García-Tomsig, N.I., Matia-González, A.M., García-Rodríguez, F.M., and Jiménez-
897 Zurdo, J.I. (2021). Synthetase of the methyl donor S-adenosylmethionine from nitrogen-fixing α-rhizobia
898 can bind functionally diverse RNA species. RNA Biology *18*, 1111–1123.
899 10.1080/15476286.2020.1829365.

900 53. Britos, L., Abeliuk, E., Taverner, T., Lipton, M., McAdams, H., and Shapiro, L. (2011). Regulatory
901 Response to Carbon Starvation in Caulobacter crescentus. PLOS ONE *6*, e18179.
902 10.1371/journal.pone.0018179.

903 54. Cabrera, J.E., Cagliero, C., Quan, S., Squires, C.L., and Jin, D.J. (2009). Active Transcription of
904 rRNA Operons Condenses the Nucleoid in Escherichia coli: Examining the Effect of Transcription on
905 Nucleoid Structure in the Absence of Transertion. Journal of Bacteriology *191*, 4180–4185.
906 10.1128/JB.01707-08.

907 55. Queiroz, R.M.L., Smith, T., Villanueva, E., Marti-Solano, M., Monti, M., Pizzinga, M., Mirea, D.-
908 M., Ramakrishna, M., Harvey, R.F., Dezi, V., et al. (2019). Comprehensive identification of RNA–protein
909 interactions in any organism using orthogonal organic phase separation (OOPS). Nat Biotechnol *37*, 169–
910 178. 10.1038/s41587-018-0001-2.

911 56. Shchepachev, V., Bresson, S., Spanos, C., Petfalski, E., Fischer, L., Rappsilber, J., and Tollervey, D.
912 (2019). Defining the RNA interactome by total RNA-associated protein purification. Molecular Systems
913 Biology *15*, e8689. 10.15252/msb.20188689.

914 57. Hentze, M.W., Castello, A., Schwarzl, T., and Preiss, T. (2018). A brave new world of RNA-binding
915 proteins. Nat Rev Mol Cell Biol *19*, 327–341. 10.1038/nrm.2017.130.

916 58. Riback, J.A., Katanski, C.D., Kear-Scott, J.L., Pilipenko, E.V., Rojek, A.E., Sosnick, T.R., and
917 Drummond, D.A. (2017). Stress-Triggered Phase Separation Is an Adaptive, Evolutionarily Tuned
918 Response. Cell *168*, 1028-1040.e19. 10.1016/j.cell.2017.02.027.

919 59. Evinger, M., and Agabian, N. (1977). Envelope-associated nucleoid from Caulobacter crescentus
920 stalked and swarmer cells. Journal of Bacteriology *132*, 294–301. 10.1128/jb.132.1.294-301.1977.

921 60. Schrader, J.M., and Shapiro, L. (2015). Synchronization of Caulobacter Crescentus for
922 Investigation of the Bacterial Cell Cycle. JoVE (Journal of Visualized Experiments), e52633.
923 10.3791/52633.

924 61. Cronin, R.M., Ferrell, M.J., Cahir, C.W., Champion, M.M., and Champion, P.A. (2022). Proteo-
925 genetic analysis reveals clear hierarchy of ESX-1 secretion in Mycobacterium marinum. Proceedings of
926 the National Academy of Sciences *119*, e2123100119. 10.1073/pnas.2123100119.

927 62. Vernon, R.M., Chong, P.A., Tsang, B., Kim, T.H., Bah, A., Farber, P., Lin, H., and Forman-Kay, J.D.
928 (2018). Pi-Pi contacts are an overlooked protein feature relevant to phase separation. eLife *7*, e31486.
929 10.7554/eLife.31486.

930 63. Ducret, A., Quardokus, E.M., and Brun, Y.V. (2016). MicrobeJ, a tool for high throughput
931 bacterial cell detection and quantitative analysis. Nat Microbiol *1*, 1–7. 10.1038/nmicrobiol.2016.77.

932 64. Postma, M., and Goedhart, J. (2019). PlotsOfData—A web app for visualizing data together with
933 their summaries. PLOS Biology *17*, e3000202. 10.1371/journal.pbio.3000202.

934 65. Holmes, J.A., Follett, S.E., Wang, H., Meadows, C.P., Varga, K., and Bowman, G.R. (2016).
935 Caulobacter PopZ forms an intrinsically disordered hub in organizing bacterial cell poles. Proceedings of
936 the National Academy of Sciences *113*, 12490–12495. 10.1073/pnas.1602380113.

937 66. Sherman, B.T., Hao, M., Qiu, J., Jiao, X., Baseler, M.W., Lane, H.C., Imamichi, T., and Chang, W.
938 (2022). DAVID: a web server for functional enrichment analysis and functional annotation of gene lists
939 (2021 update). Nucleic Acids Research *50*, W216–W221. 10.1093/nar/gkac194.

940 67. Romero, P., Obradovic, Z., Kissinger, C., Villafranca, J.E., and Dunker, A.K. (1997). Identifying
941 disordered regions in proteins from amino acid sequence. In Proceedings of International Conference on
942 Neural Networks (ICNN'97), pp. 90–95 vol.1. 10.1109/ICNN.1997.611643.

943 68. Bolognesi, B., Lorenzo Gotor, N., Dhar, R., Cirillo, D., Baldrighi, M., Tartaglia, G.G., and Lehner, B.
944 (2016). A Concentration-Dependent Liquid Phase Separation Can Cause Toxicity upon Increased Protein
945 Expression. Cell Reports *16*, 222–231. 10.1016/j.celrep.2016.05.076.

946 69. Saar, K.L., Morgunov, A.S., Qi, R., Arter, W.E., Krainer, G., Lee, A.A., and Knowles, T.P.J. (2021).
947 Learning the molecular grammar of protein condensates from sequence determinants and embeddings.
948 Proceedings of the National Academy of Sciences *118*, e2019053118. 10.1073/pnas.2019053118.

949

Figure 1

A. BR-body enrichment assay

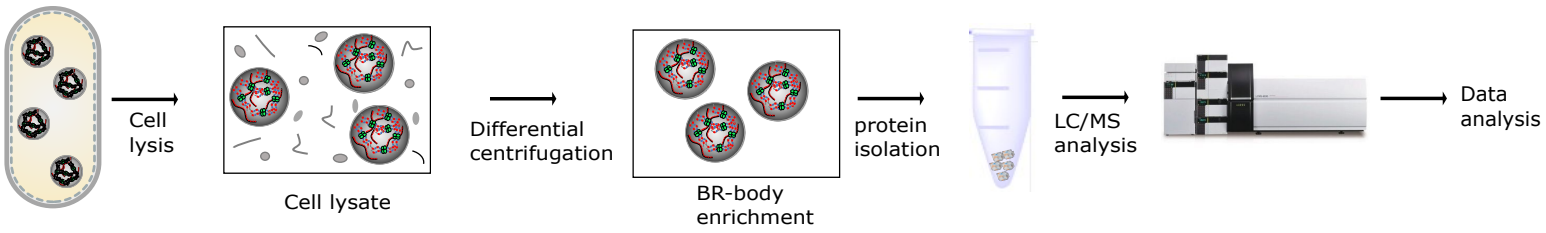

B.

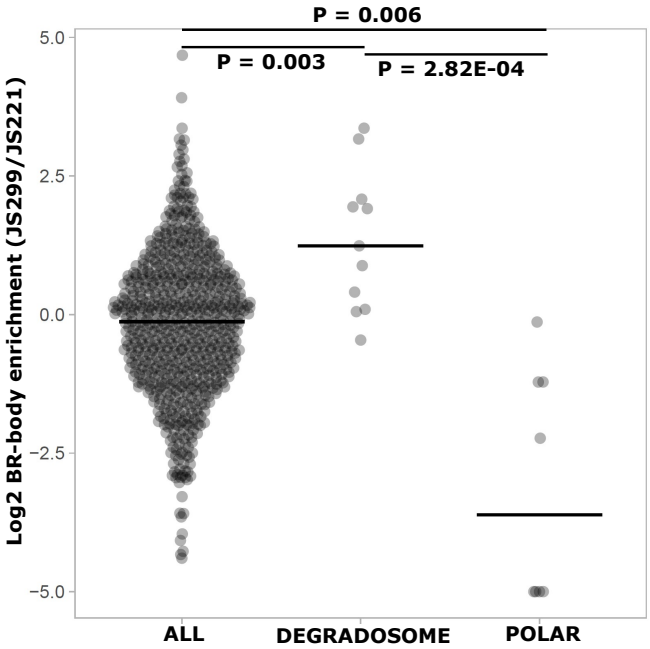

Enriched	Number of proteins	p-value
Cytoplasm	32	9.40E-11
Depleted		
Membrane	160	3.90E-23
Transmembrane	126	2.30E-12
Cell inner membrane	33	3.00E-12
Transmembrane helix	121	3.80E-11
Cell membrane	40	4.30E-11
Cell outer membrane	7	1.30E-03
Cell wall	5	6.40E-02

Enriched	Number of proteins	p-value
RNA Binding	14	9.00E-07
ATP Binding	19	8.80E-03
RNA Degradation	5	9.90E-03
GTPase Activity	5	3.80E-03

C.

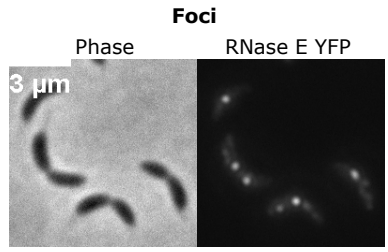

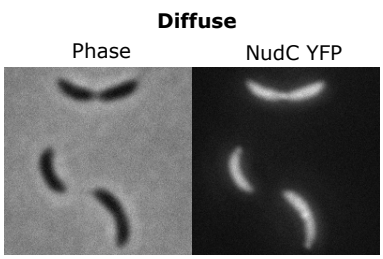

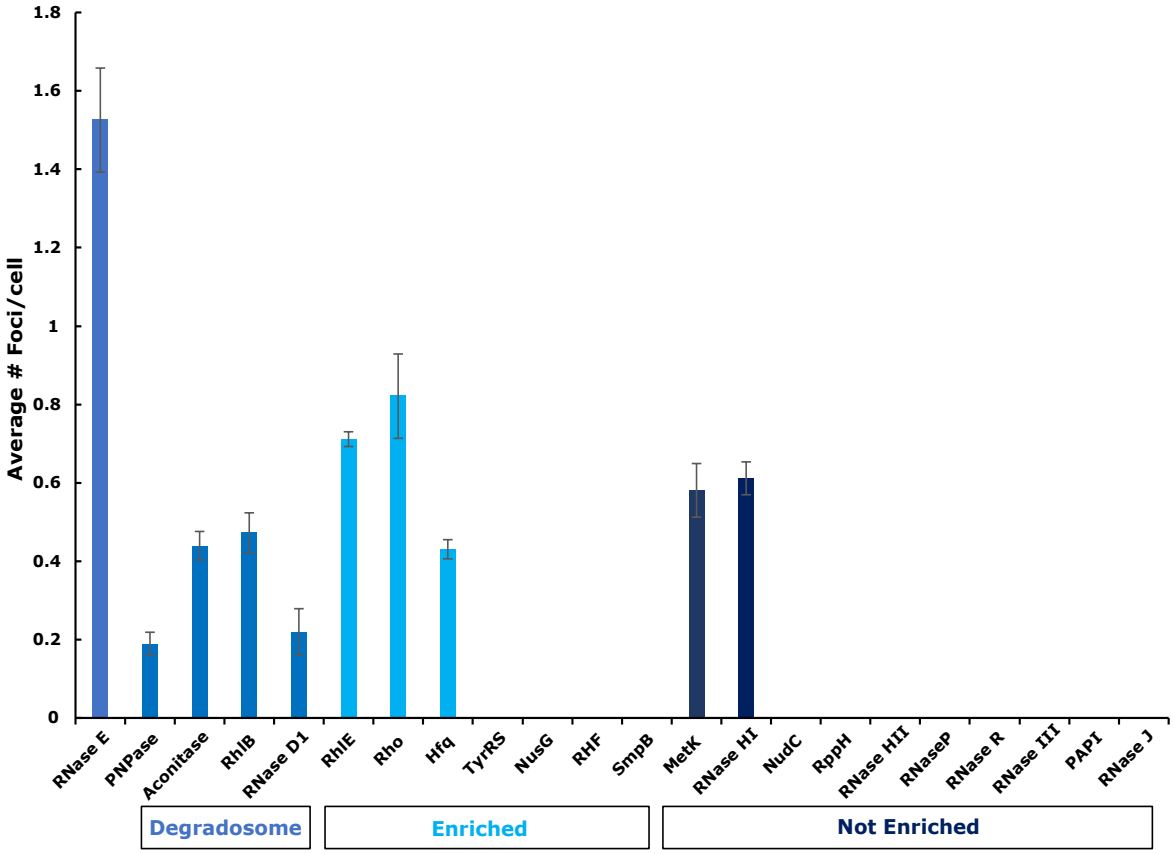

Figure 2

A.

B.

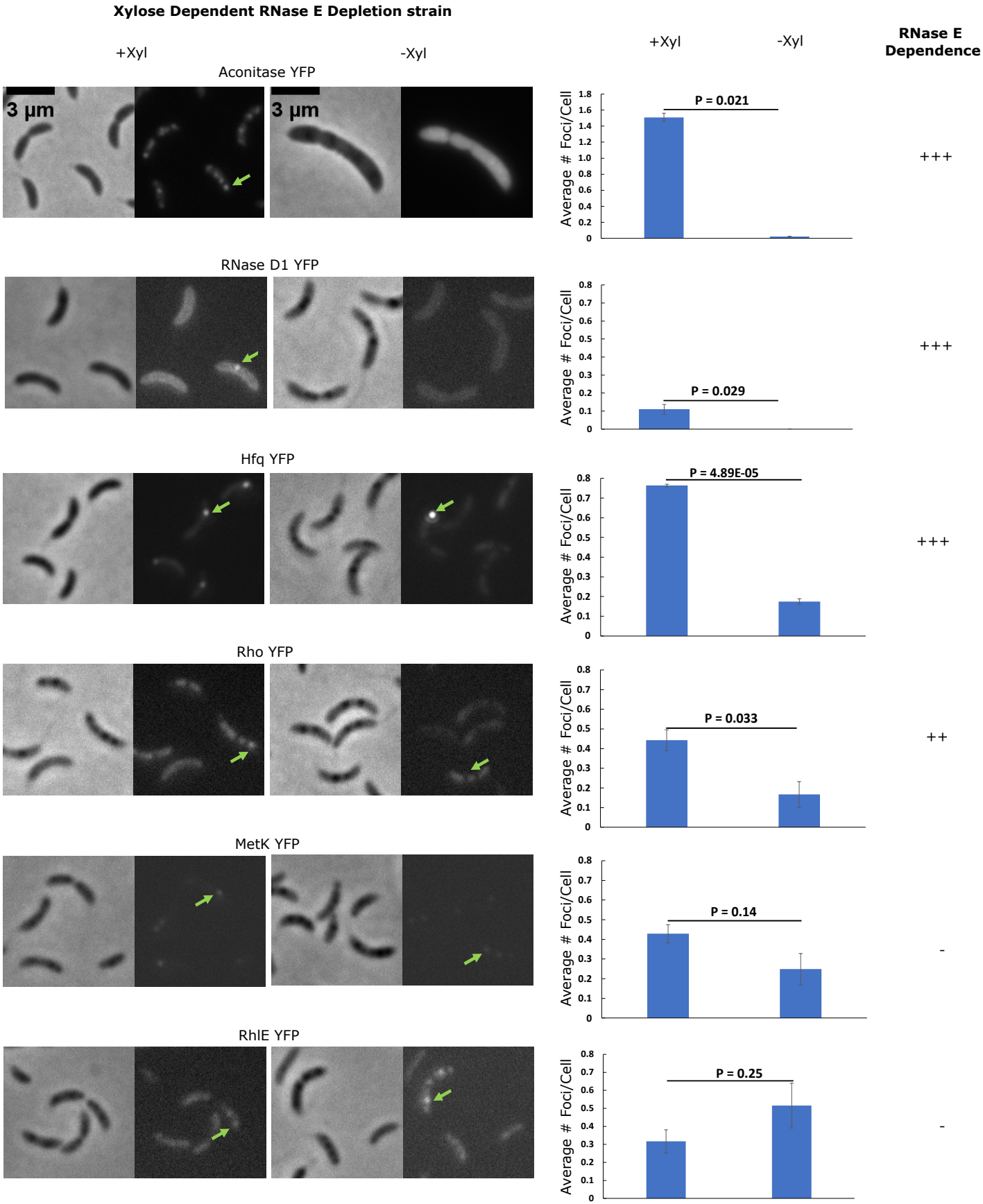

A.

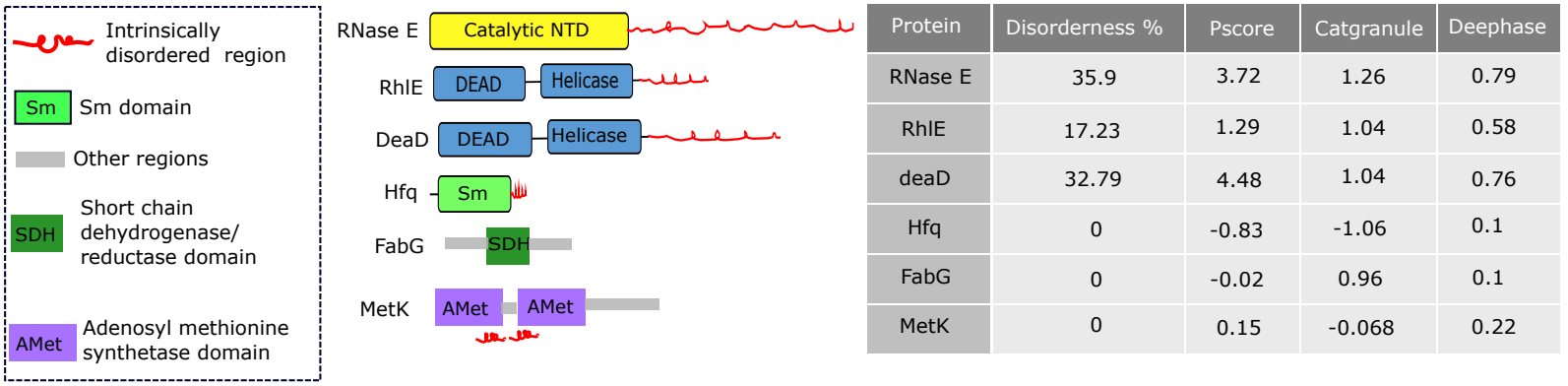

Protein	Disorderness %	Pscore	Catgranule	Deephase
RNase E	35.9	3.72	1.26	0.79
RhlE	17.23	1.29	1.04	0.58
deaD	32.79	4.48	1.04	0.76
Hfq	0	-0.83	-1.06	0.1
FabG	0	-0.02	0.96	0.1
MetK	0	0.15	-0.068	0.22

B.

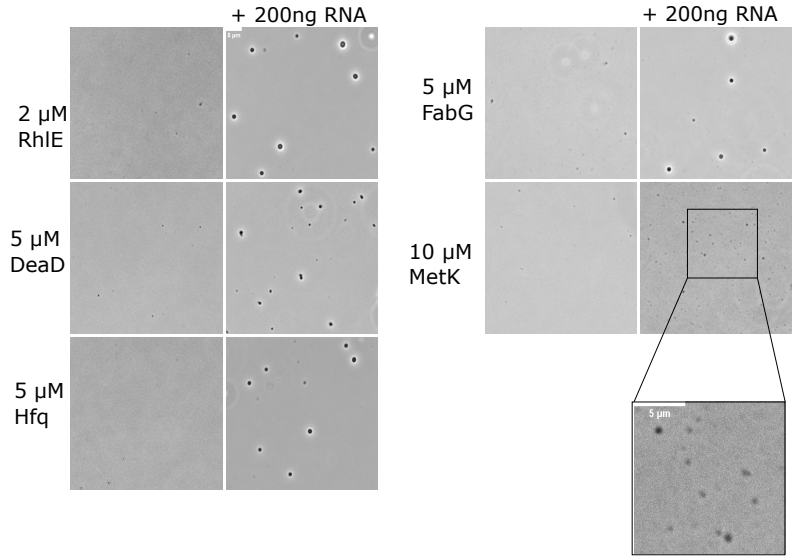

C.

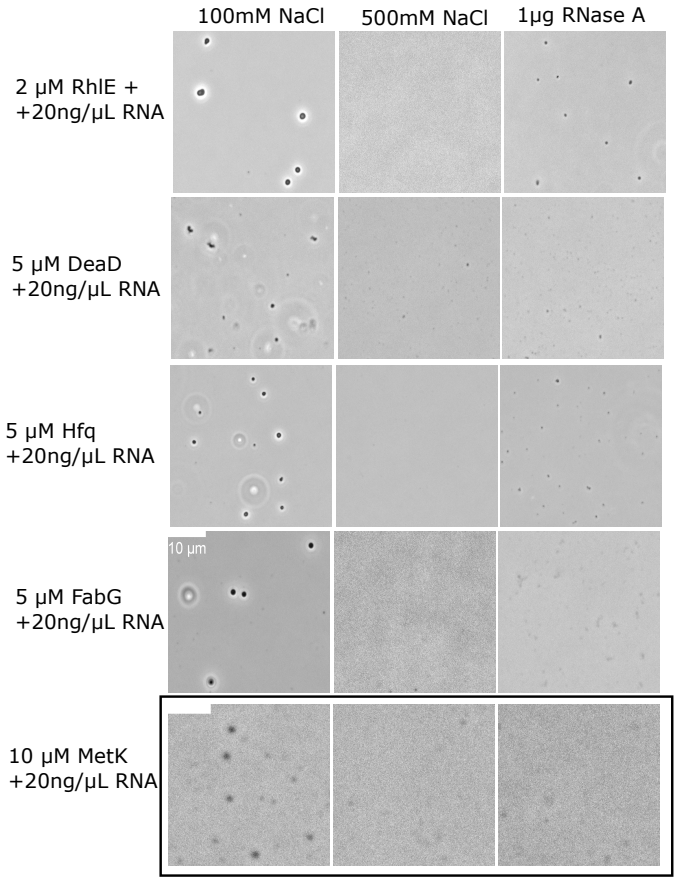

Figure 4

A.

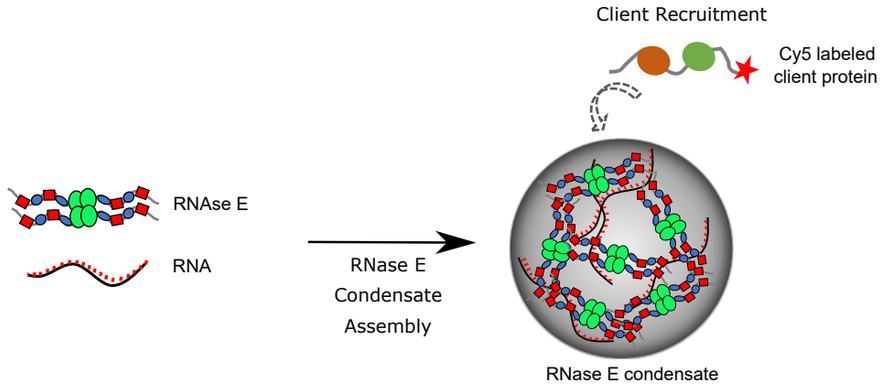
Client Recruitment
Cy5 labeled
client protein
RNAse E
RNA
RNase E
Condensate
Assembly
RNase E condensate

B.

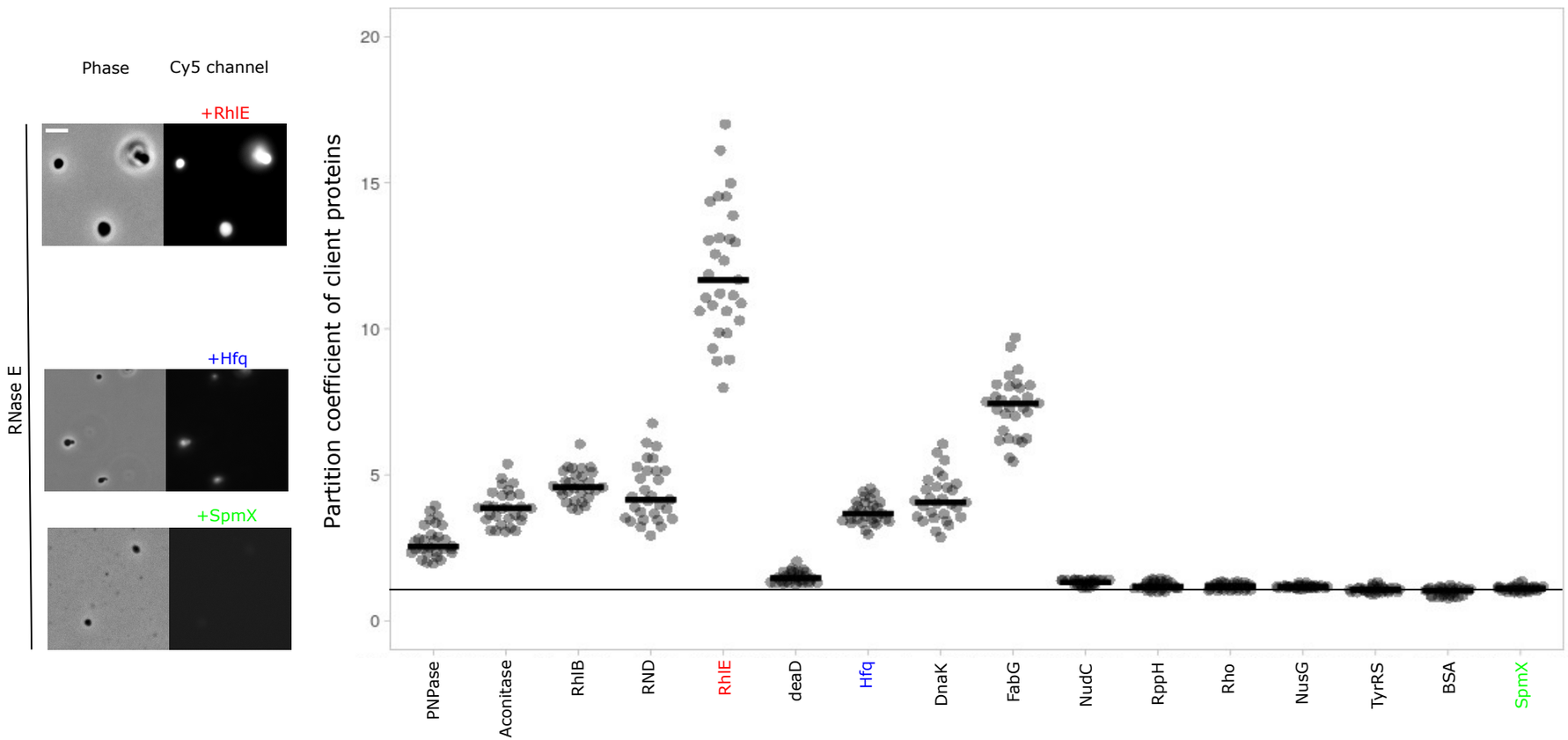
Phase
Cy5 channel
RNase E
+RhlE
+Hfq
+SpmX
Partition coefficient of client proteins
20
15
10
5
0
PNPase
Aconitase
RhlB
RND
RhlE
deaD
Hfq
DnaK
FabG
NudC
RppH
Rho
NusG
TyrRS
BSA
SpmX

Figure 5

A.

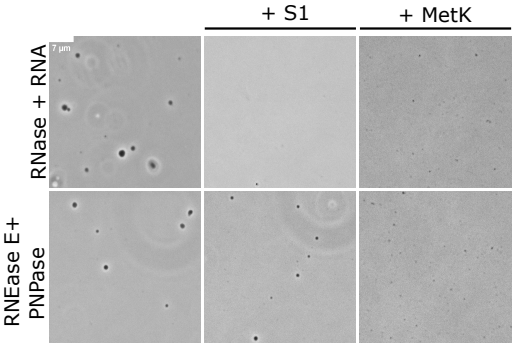

B.

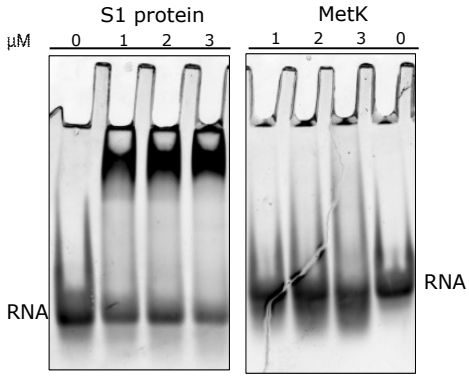

C.

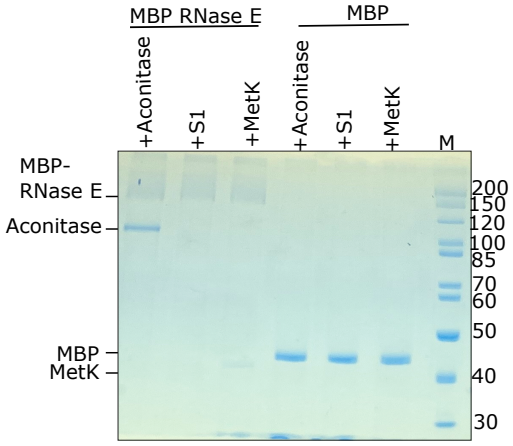

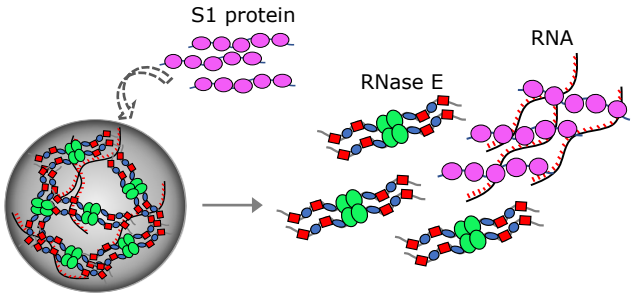

S1 protein dissolution occurs via RNA binding

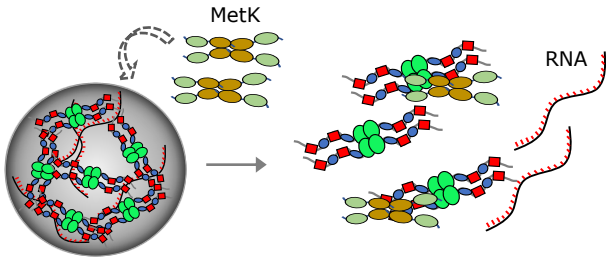

MetK dissolution occurs via RNase E binding

D

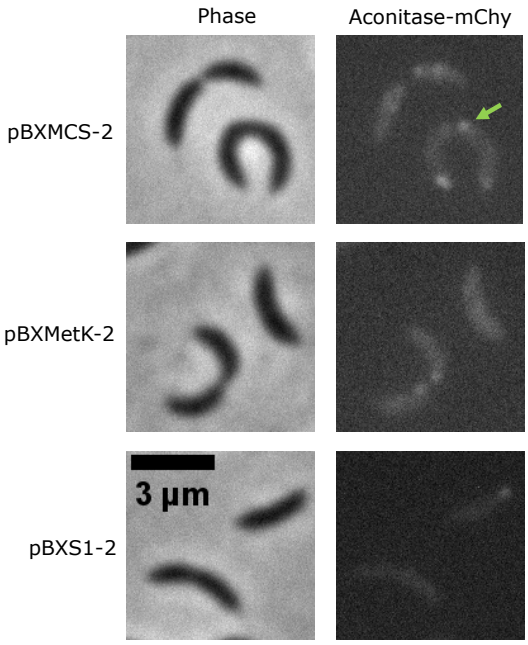

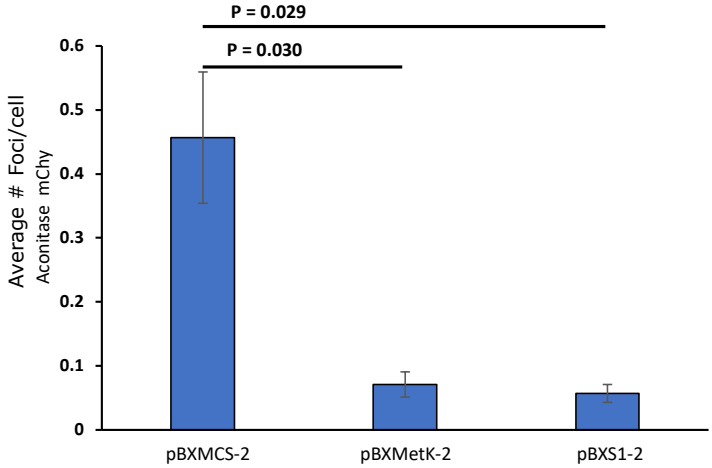

A.

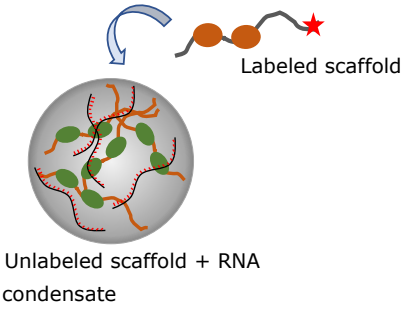

+RNA Scaffold	Labeled Scaffold: RNase E	RhlE	DeaD	Hfq	FabG
RNase E	X	11	1.5	7.5	3.8
RhlE	1.6	X	1.5	2.5	2.5
DeaD	1.7	7.6	X	3.3	2.6
Hfq	ND	4.3	1.8	X	2.4
FabG	1.9	7.4	1.5	3.4	X

Partition Coefficient: 15 High, 10, 5, 1 Low

B.

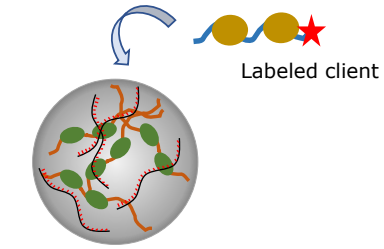

-RNA Scaffold	Labeled client: RhlB	PNP	Aco	RND
RNase E	4.7	2.6	4	4
RhlE	1.0	1.0	1.0	1.0
DeaD	1.5	1.5	1.5	1.5
Hfq	2.3	1.7	2.5	1.7
FabG	1.5	1.7	1.5	1.6

C.

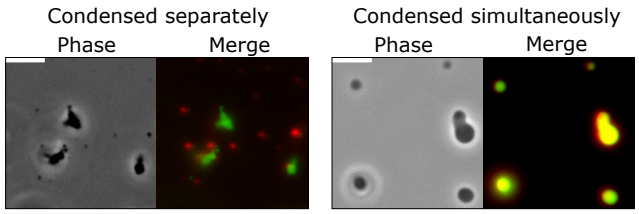

D.

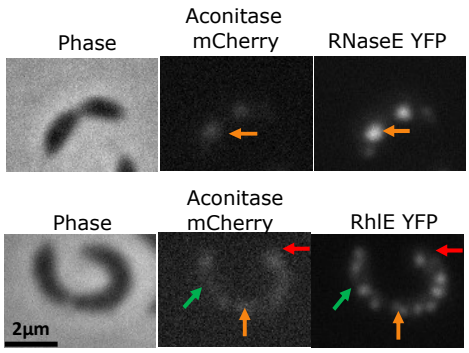

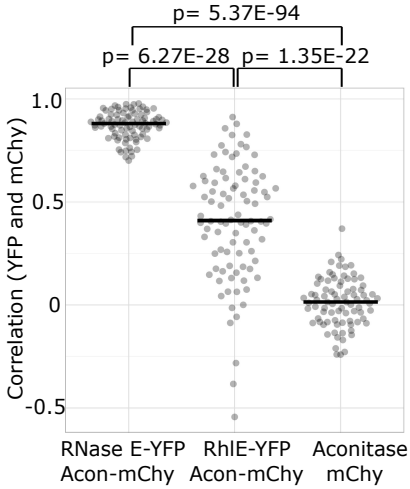

E.

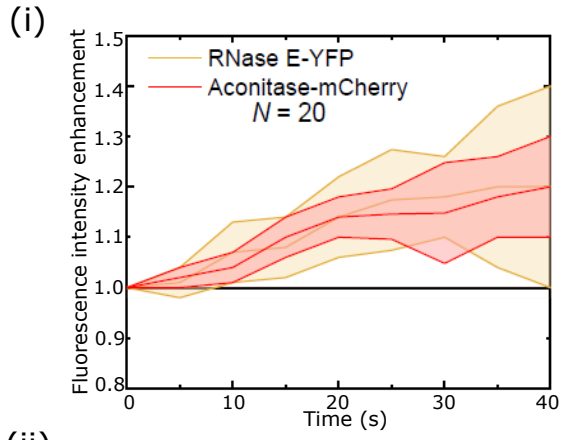

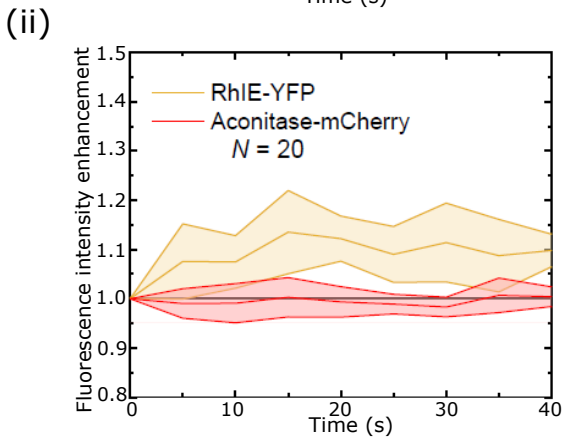

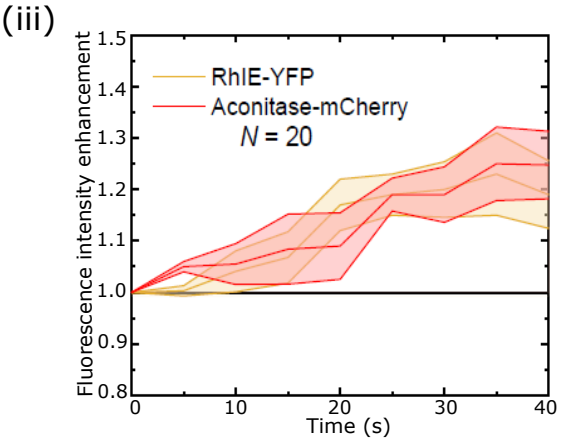

Figure 7

A.

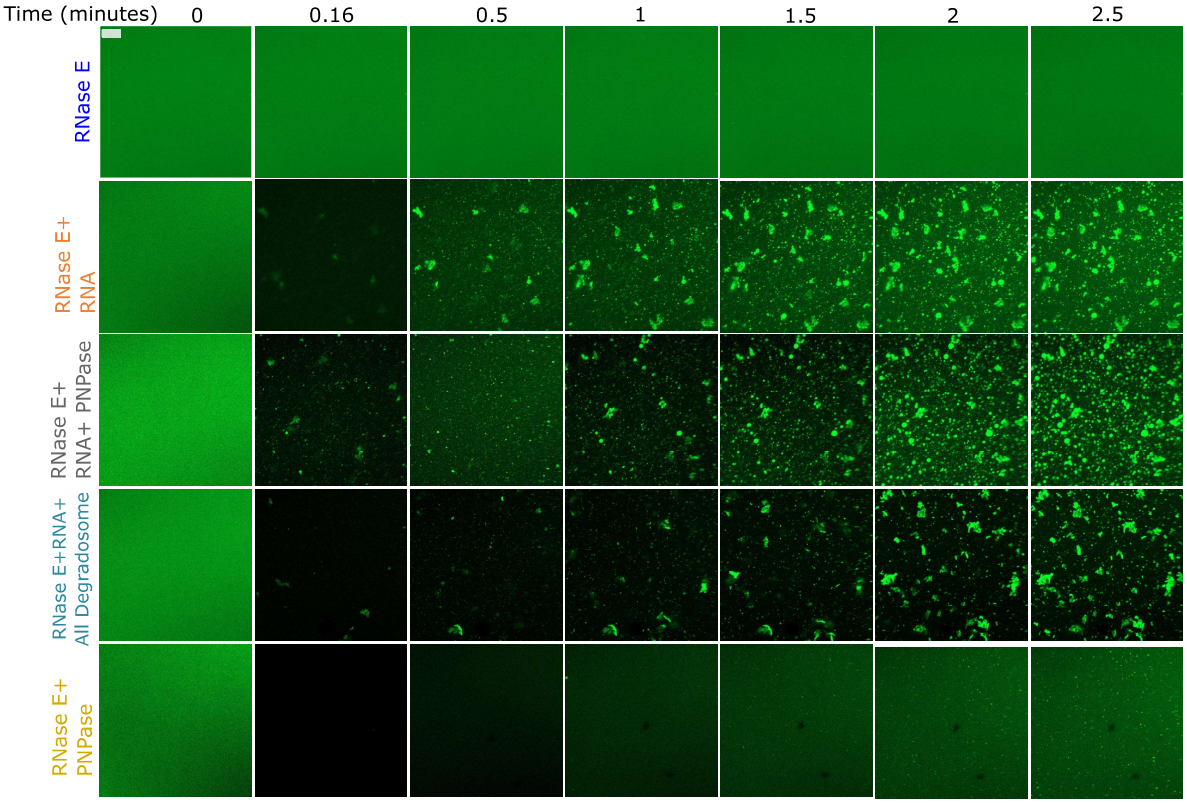

B.

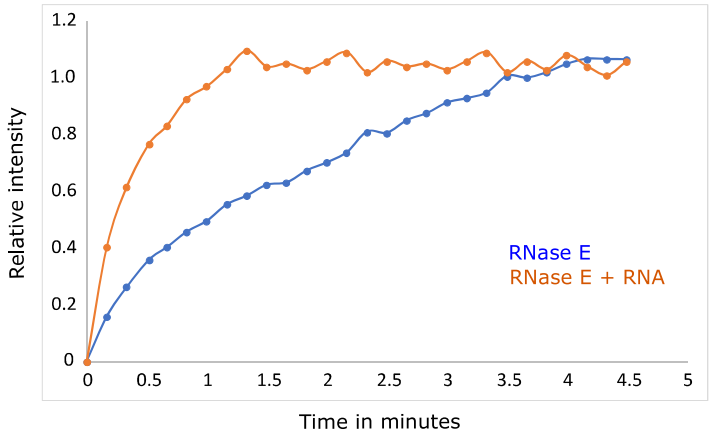

C.